Designing an Optical Device for Measuring Surface Roughness

Final Report
15 December 2009

Kyle Antonini
Derek Geiger
Ryan Orizondo
Tiago Szvarca

University of Michigan

Department of Mechanical Engineering

ABSTRACT

Reliable measurement of surface roughness (R_a) is critical to quality control in a wide range of manufacturing processes. The purpose of this project is to design a proof-of-concept device for non-invasive measurement of R_a. Through the preliminary design process for this device, we concluded that the device must be low-cost, accurate, and safe to implement. By decomposing our device into its critical sub-functions, we were able to generate a large pool of concept designs. With experimentation and objective evaluation, we narrowed this pool down to an alpha design incorporating a vertical orientation, purple LED and webcam. The final prototype was manufactured with rapid prototyping. We also made considerations for altering this design for marketability. The prototype was completed and successfully validated on schedule and under budget.

TABLE OF CONTENTS

EXECUTIVE SUMMARY……..3

INTRODUCTION AND BACKGROUND…..……...……4

SPECIFICATIONS……...……...……7

CONCEPT GENERATION……...……..9

EXPERIMENTATION…….....11

CONCEPT SELECTION……..15

ALPHA DESIGN…….... 17

PARAMETER ANALYSIS AND FURTHER EXPERIMENTATION...…… 18

FINAL PROTOTYPE...…… 25

FINAL DESIGN CONSIDERATIONS……...30

VALIDATION TESTING AND RESULTS…… 33

DESIGN CRITIQUE AND RECOMMENDATIONS…….. .36

CONCLUSIONS……..……... 38

ACKNOWLEDGEMENTS…….. ...38

REFERENCES…….....39

APPENDIX A…….... 41

APPENDIX B…….... 42

APPENDIX C…….... 43

APPENDIX D…….... .51

APPENDIX E…… 52

EXECUTIVE SUMMARY

Reliable measurement of surface roughness (R_a) is critical to quality control in a wide range of manufacturing processes. The purpose of this project is to design a proof-of-concept device for non-invasive measurement of R_a. This device must capture the intensity of visible light reflected by a set of controlled surfaces and correlate this value to a measurement of R_a.

In early stages of the design process we evaluated our customer needs, benchmarked the success of current devices against these needs, and linked them to quantifiable engineering specifications (see Table 2, page 8). With preliminary experimentation regarding the light source and relative orientation we were able to narrow our design solutions to an alpha design (Page 17). This alpha design showed initial promise, but was limited by the difficulty of standard image analysis. We then performed extensive experimentation to develop a standard algorithm for image analysis and evaluate the sensitivity of our device to changes in working distance and relative working angle (Page 18). We finalized our image analysis procedure,and determined that the vertical orientation of our design is forgiving in terms of working distance but sensitive to changes in working angle.

These experimental results led directly to the detailed design of our prototype device. This prototype uses the vertical orientation and purple LED of the alpha design, but has some new features to ensure more robust performance. The prototype has a pellicle beamsplitter rather than a cubic beamsplitter, eliminating ghost images, and also has separate doors for the main compartment to keep the pellicle mirror as isolated as possible. We chose to fabricate the prototype with the Dimension FDM Elite 3-D printer. This rapid prototyping allows us to ensure the beamsplitter is set at a 45º angle relative to the light source, and reduces machine time while simplifying assembly. The user interface was created in LabVIEW, and the algorithms used analyzed the images based on light intensity and shape.

We also developed a validation plan to ensure that our device would meet the customer requirements stated at the beginning of the project. We have explicit tests to determine the device's ability to discern R_a under different conditions (Page 33), and we also evaluated the cost and invasiveness of the device. The completed prototype was assembled easily, with most of the parts press-fitted, save for two screws used to fasten the beamsplitter to its frame. We ran it through our validation procedure and it met passed all tests under normal operating conditions. The device proved to be capable of measurement with a ±2mm shift in working distance or a ±2° tilt without recalibration, and it can measure accurately from 1mm to 30mm from the surface of interest with recalibration.

We were most proud of our device's ability to accurately and reliably make its measurements with a high level of robustness. We were also happy that we took the objective of "test stand" a step further and made the initial move toward a marketable design that was small and easy to assemble. We felt that we could better improve our device if we had a lens to change our image data and zoom in upon our small area of interest for better resolution of the light reflection pattern.

If given more time with our device, we would add an automated calibration procedure to the LabVIEW interface that automatically thresholds light intensity into the proper output data, given images of known R_a. This takes away any advanced calibration knowledge that the user needs to operate the device.

INTRODUCTION AND BACKGROUND

The University of Michigan's Engineering Research Center for Reconfigurable Manufacturing Systems tasked our group with designing a device that can accurately and reliably measure the roughness (R_a) of a specific set of ground metal surfaces. This could not be completed without a thorough investigation into the industrial applications of surface roughness measurement and the current methods of making such a measurement.

Industry Applications

Surface roughness is a key quality indicator for manufacturing processes in a wide variety of industries. Nano-scale characterization of surfaces is critical to understanding the electrical performance of etched silicon films, and the dissolution behavior of pharmaceutical tablets [1, 2]. Micro-scale differences in R_a impact the performance and lifetime of automotive engine and drive-train components, as well as the performance of blades in turbine engines [3, 4]. Micro-characterization of surfaces is also important in the extensive industry of protective coatings for metals [5, 6].

In the particular case of metal coating, a device capable of inline inspection of pre- and post-process surface roughness could be a breakthrough competitive advantage. In the international shipping industry, marine engineers use anti-fouling coatings on the surface of hulls to prevent increases in drag due to the adhesion of fouling organisms [5]. For perspective, an increase in 5 μm of micro-roughness of a cargo ship hull can increase the overall drag by ~4% [5]. The international shipping industry expends $380 billion in freight rates and contributes 10.12 Tg (Tg = 10^9 kg) of NOx and 8.48 Tg of SOx per year to the atmosphere [5]. Given an industry of this scale, small percentage improvements in the quality of surface coatings can have profound effects on the environmental impact and total delivered cost of goods. A device capable of providing accurate, reliable feedback to the quality control system of an anti-fouling coating process can have a significant, positive impact on the shipping industry and the environment.

We are working to prototype an inexpensive device capable of quickly and safely measuring the micro-scale R_a of surfaces of interest in a variety of manufacturing processes. If successful, the resulting proof-of-concept prototype will provide breakthrough quality control feedback to any industry that is performance-dependent on the surface roughness of materials. The next step in developing this system is to understand the fundamental phenomena of optical surface roughness measurement.

Fundamental Technology Research

In order to understand the scientific fundamentals of the device, we explored current literature on noncontact surface roughness measurement [7-12]. The most prevalent method in optical surface measurement utilizes the physics of scattered light on rough surfaces. Current devices use light from a wide spectrum of wavelengths, including infrared and ultraviolet [7]. The Beckmann-Kirchoff Scatter Model [8], which describes the wave interaction of light with rough, opaque surfaces, was continually referenced as one of the governing principles of this application.

From this research, we have concluded that the resolution of optical devices is dependent upon the wavelength of the light source. Large wavelength sources can be blind to the effect of small deviations in the surface, so we have to select an appropriate wavelength to achieve our desired resolution [9]. It is next necessary to explore how well other current technologies make use of these scientific principles.

Benchmarking

Many surface roughness measurement devices currently exist in industry. There are three main categories that we will analyze on a closer scale: stylus-type contact measurement instruments, non-contact laser measurement devices, and non-contact white-light measurement devices. All three are currently used in a

variety of applications to analyze surface roughness—among other surface properties—of varying types of material.

Stylus Method

Stylus-type contact measurement devices are the most primitive type of device used to measure surface roughness. These devices operate by moving a small probe across the test surface to detect variations in height. This class of devices has many disadvantages, including speed of measurement, invasive nature, and tendency to be highly affected by surface abnormalities. For this type of device to accurately work, the device's probe must remain in contact with the sample surface. In some cases, the load this probe exerts on the surface can cause destructive plastic deformation. If the speed at which the stylus moves across the surface is too high, the probe can lose contact with the surface, distorting the output. For this reason, accurate surface measurement with this type of device is limited to a critical speed [13]. With this method of operation, a small defect in the test surface can result in an inaccurate surface roughness output.

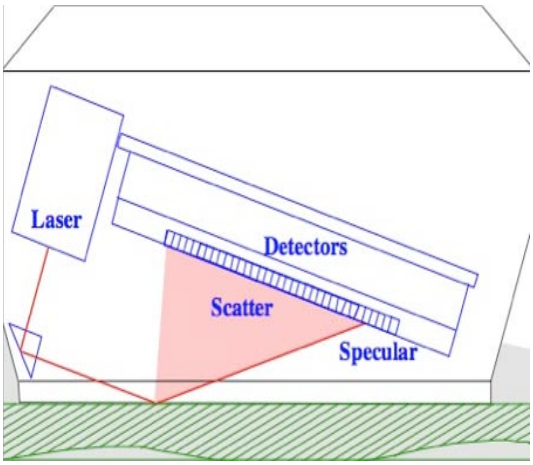

Figure 1: Non-contact laser measurement device setup.

Laser Scattering

Non-contact laser measurement devices are commonly used in many industry applications. These devices operate by emitting a concentrated laser at the test surface, either directly or via mirrors, and using detectors to measure the distribution of specular and diffused light reflected by the surface [14]. This setup is illustrated in Figure 1. The major disadvantages of this class of devices include its limited working distance to the test surface, the potential dangers of high energy lasers, and the laser's inability to examine large spans of surface. Although many laser measurement devices overcome this last challenge by taking multiple readings throughout a desired region, these devices still lack the ability to take a true average reading over a large area.

White Light Superposition

Non-contact surface measurement devices using white light are much less common in industry. These devices utilize the established technique of interferometry with white light along with a CCD camera to analyze surface roughness of varying materials. This process involves emitting white light on both the test surface and a high-precision reference surface, capturing these images with the CCD camera and superimposing these images in order to get an accurate analysis of the surface [15]. A diagram illustrating this setup can be seen in Figure 2. One major drawback of this particular device is the necessity of a high-precision reference surface. This can prove to be especially inconvenient when analyzing materials over a large variety of surface finishes.

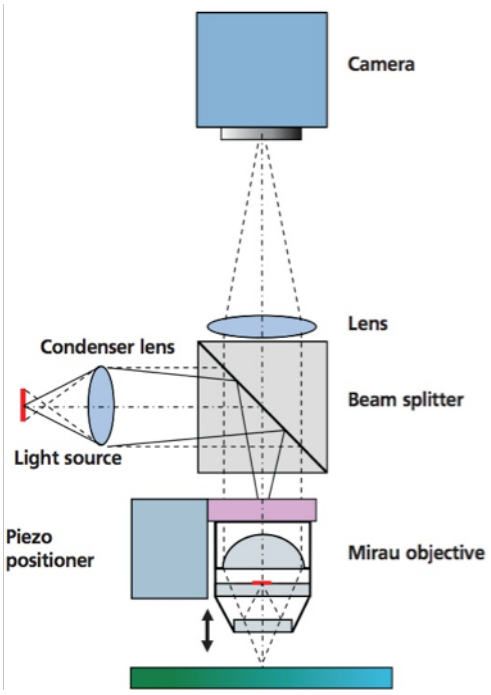

Figure 2: Non-contact white-light measurement device setup.

We decided to design a system that correlates reflected light intensity to surface roughness. To do so, it is important to understand the possible components of our system.

System Components

The three main optical components of this system are the light source, the lens choices, and the optoelectronic sensor.

Light Source

Visible light can be produced through several methods, like bulbs, LED's, and lasers. It is important to choose the right light source to meet all our needs. Each source has positive aspects and drawbacks.

A light bulb can produce the most light at the least cost. It is not a very concentrated amount of light, though, and it will produce a lot of excess light that is of no use to us. It is also a very inefficient use of power, and it can produce an unnecessary amount of excess heat.

An LED is a more efficient source of light, and it is available in much more concentrated arrangements, which will better allow us to point the light at specific areas of interest. It is also widely available in different colors, which is very important to our accuracy success, because shorter wavelength light is capable of detecting higher resolutions on the surface of interest.

Lasers are also very attractive sources of concentrated light, but for our application, they are much too concentrated. We want to be able to inspect over an area of 200 mm^2, but lasers look at far too specific points. Their precision also makes them prone to error if not perfectly aligned at the proper distance and orientation.

Lens

Lenses will be essential to our device, because they will help direct the light where we want it to go. Two important kinds of lenses that we will consider using are converging (convex) lenses and collimating lenses. A convex lens will take incident light and concentrate it onto a smaller area. This requires more precise adjustment, because the light through the lens gets focused at a specific distance away from the lens. A collimating lens "straightens" out the incident light, transmitting it in a columnar fashion. This is more versatile, because it does not require a specific focal distance for set-up, and it will keep the focus of the image over a wider range of distances from the lens.

Optoelectronic Sensor

There are two common types of receptor devices we could use to convert light to electronic signals—charge-coupled devices (CCD's) and CMOS Active Pixel Sensors (APS's).

A CCD uses a layer of silicon as a photoactive region, made up of tiny capacitors, placed upon a transmission region. When light is incident upon the photoactive region, the capacitors are charged in proportion to the intensity of the light upon them. A control circuit then transfers the charge from each capacitor to the neighboring one, until reaching the end of the array, where the charge is dumped into a charge amplifier and converting to a voltage and stored in memory.

A CMOS APS is an integrated semiconductor circuit in which each individual pixel contains a photosensor and active amplifier. The APS's combination of both sensing and processing into the same integrated circuit makes for less image lag than a CCD. It will also consume less power and can generally be fabricated more cheaply than a CCD.

Because the success of our light acquisition process is based upon light intensity detection, it is not necessary to worry about the image quality or lag issues that distinguish the different kinds of light

sensors. It will be most important to obtain a sensor that can accurately distinguish slight changes in magnitude of light intensity.

SPECIFICATIONS

Customer Requirements

In order to gain insight into how our device could improve upon current similar devices, we turned to our customers, Dr. Hagay Bamberger and Dr. En Hong. Dr. Bamberger and Dr. Hong are researchers in the Mechanical Engineering Department at the University of Michigan. During these meetings, Dr. Bamberger and Dr. Hong stressed the industry's need for a surface measurement device with the following attributes:

- Easily integrated to assembly line / factory setting
- Accurate and resolved over a practical range of R_a values
- Able to analyze larger sample region than current devices

With these specific device requirements outlined by our customers, we analyzed parts of existing designs that we could improve upon as well as parts that did not need to be as acute for our purposes. We separated these customer needs into well defined requirements (shown below in table 3). Each requirement was given an importance rating of 1 to 5 which we later used in the Quality Functional Deployment diagram (QFD – see appendix B) to rank our engineering parameters.

Table 1: Relative Importance of Customer Requirement

Customer Requirement	Relative Weight
Capable of Discerning between R_a's of 0.1, 0.2, 0.4, 0.8, 1.6 µm	5
Safe for User and Surrounding Environment	5
Minimized Invasiveness	5
Capable of Measuring a sample of area 200 mm^2	5
Repeatable	4
Completes Measurements Quickly	4
Easily Operable User Interface	4
Low Cost of Implementation	4
Durable	3
Easily Movable / Portable	3
Aesthetics	1

A major concern for our customer was to use this device in a factory assembly line setting. In order to meet this request, our device needs to be quick, non-invasive, safe, easily operable, durable, and portable. Many existing devices are bulky and use high-energy lasers that can present potential dangers in a factory setting. Our customer is concerned with the device's accuracy but also requires that the resolution be catered to its specific application. We aim to build a device that can discern between R_as of 0.1, 0.2, 0.4, 0.8, and 1.6 µm. Existing devices are capable of measuring the surface roughness of a material to an extremely high resolution but at a high cost.

For the specific application of inline roughness measurement, a moderate resolution is sufficient. The final concern for our customer was to easily analyze large sample regions. Existing laser devices can only analyze a very concentrated area. Although these devices can be set up to take multiple readings throughout a region to produce an average reading, we aim to design a device that directly measures the average of an entire region. In our case, the regions of interest are 1cm by 2cm test surfaces that our customer already owns. At this point, after reaching an understanding of the customer requirements, our team set out to assign quantifiable engineering parameters to meet these customer needs.

Engineering Parameters

We generated a list of engineering parameters that will affect this system. Using the correlation matrix in the QFD (appendix B), we quantified how much each engineering parameter related to each customer need. By multiplying these "correlation coefficients"—which were given a value of 1, 3, or 9—and the importance rating of each customer need, we were able to rank the importance of each engineering parameter for our design. Table 4 shows this ranking.

Table 2: Relative Importance of Our Engineering Parameters

Parameter	Rank	Target
Light source dispersion	1	TBD
Optical sensor resolution	2	High
Distance from sample	3	1-10 mm
Light wavelength	4	380-750 nm
Light intensity	5	TBD
Measurement time	6	3 sec
Steps in operation	8	1 step
Sensor signal-to-noise ratio	9	10
Weight	10	1 kg
Length	11	150 mm
Width	11	150 mm
Height	13	400 mm
Angle of incidence of light	13	TBD

As a result, we noticed that the method of delivering light is the most important factor to consider. Light dispersion affects the accuracy and repeatability of measurements. It also affects the versatility of the sample areas it can measure and the cost. Unlike current systems that average multiple readings of small areas, we intend to disperse the light over a larger area and take a single reading. This will reduce the complexity of the software involved and drastically reduce the time of measurement.

The optical sensor is also a crucial part of our device. The sensor resolution ranked second in our analysis, as it was strongly correlated to the resolution of our readings, the precision of readings, and the cost. Our choice of optical sensor must balance adequate sensor resolution with low cost. As we have mentioned before, current products on the market are very precise but also very expensive. Thus, in order to create market share for our product, we will prioritize reducing cost at the expense of reducing resolution in the readings.

The distance from the light source to the sample is also a parameter of great importance. It affects the accuracy, repeatability, and resolution of measurements. It is critical to have sufficient clearance between the device and the sample to be feasibly implemented in a dynamic assembly line.

The wavelength and intensity of the light source are also of great importance. The wavelength will have bearing on the accuracy and resolution of readings, as well as the safety of the device. Some wavelengths—such as ultraviolet—can have harmful side effects. Our light source must have a wavelength that is safe and provides adequate resolution on the surface [9].

The design parameters highlighted above will be the most important during the coming preliminary design process. However, other considerations such as measurement time, geometry, weight and number of operational steps will also be important when designing the device. These will have implications in product implementation, product durability, safety, and user friendliness.

CONCEPT GENERATION

Functional Decomposition

After defining the critical customer requirements and engineering specifications of our device it was pertinent to define the necessary functions that our device *must* perform to meet these requirements. To accomplish this we generated a functional decomposition, and have included a visual representation of this for our device in Figure 3 below.

Figure 3: Functional Decomposition Diagram

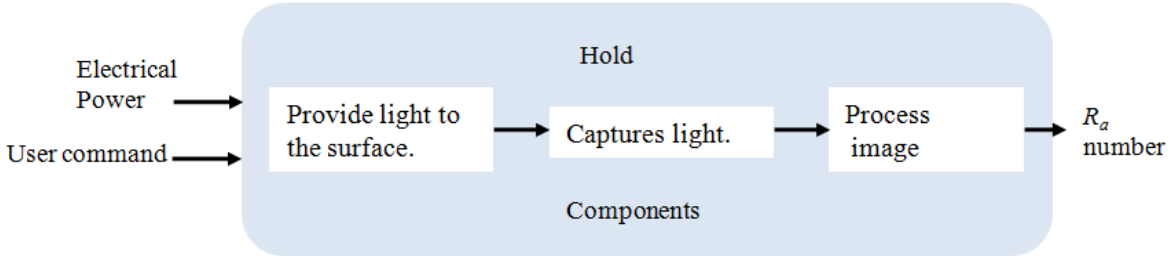

The primary function of our device is to receive human activation and output a measurement of R_a. Our device is constrained to accomplish this by measuring the intensity of reflected light, so we included the three sub-functions of: providing light to the surface (source), capturing reflected light (sensor), and processing the captured image. It is important to note that an additional constraint on our device is that it must be a stand-alone entity, so we have included the over-bearing function of holding the components together. While this function may seem trivial, the orientation of the source with respect to the sensor is a critical aspect of our design, and is intimately dependent on the way in which we fix the components.

The final item to note from the functional decomposition is a general understanding of the flow of energy and information. While providing light, we create the by-products of heat and scattered light, the handling of which has implications on the overall safety of the device. This functional decomposition summarizes the essential tasks that our device must complete, and the fundamental inputs and outputs involved with those tasks. By successfully defining the functions of our device, we can generate a collection of concept designs to accomplish each individual function.

Concept Generation

After decomposing our problem statement into an ordered list of necessary functions, we generated multiple concept designs to complete those functions. To generate these designs we combined ideas from existing literature, discussion with our customers (Dr. Hagay Bamberger and Dr. En Hong), interviews with industry experts at Picometrix (Irl Duling and Jeff White), and independent brainstorming. From these sources we decided that the principal differentiating characteristic of our concept designs would be the orientation of the light source and optical sensor with respect to the surface of interest. This section details the strengths and weaknesses of our three principal orientations. Inside each principal orientation we developed a set of sub-variations that modify the light source, optical sensor, and measuring technique.

Coaxial Source and Sensor

The first of our principal orientations has the optical sensor located directly on the axis of reflected light. A basic schematic and CAD assembly of this orientation is shown in Figure 4, with a CAD mock-up in Appendix D. One advantage of this design is that it is simple, and prior knowledge exists to suggest this orientation will be successful in resolving the roughness of the surface [16]. Since the sensor is directly aligned with the reflected light, this setup will also measure the highest reflected light intensity of any of our orientations. If the brightness of the light source is a limiting factor, then this orientation will be suitable for detecting even the weakest reflections.

Figure 4: Coaxial Sensor

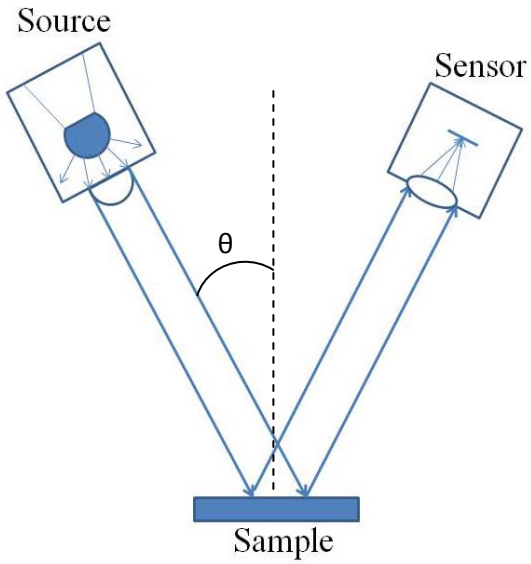

One drawback to this design is that the size of the unit is intimately dependent on the incident angle (θ) used. If it turns out that a large incident angle is beneficial to surface measurement, this design will be relatively wide in comparison to its height. Another concern raised by experts at Picometrix was that the deviations in light intensity due to the surface would be very small relative to the total measured light intensity. Jeff White of Picometrix commented that this method is analogous to "measuring the weight of the captain by measuring the weight of the ship and the captain, and subtracting the weight of the ship". This concern was the primary motivation in the generation of our second principal orientation.

Off-Axis Scattering

Figure 5: Off axis Sensor

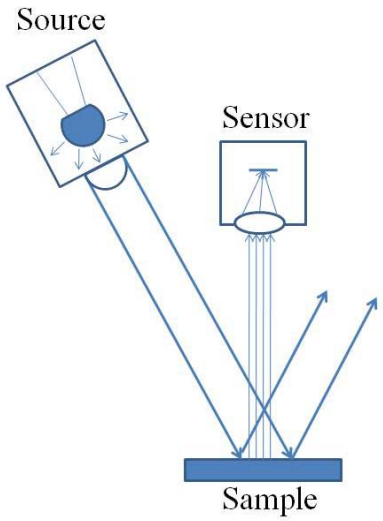

In contrast to an orientation in which the sensor receives the reflected light directly, it is also possible for the sensor to be placed off the axis of the light beam to measure the degree of scatter. In this orientation, the sensor is placed vertically above the sample, while the light source shines at a slant upon the sample. This is shown in Figure 5, with a CAD mock-up in Appendix D. The reflected light beam is not measured directly. This orientation measures only the light that scatters off-axis. In this case the intensity of light upon the sensor is greater for a rougher surface, which theoretically should have a higher degree of scatter.

The advantage of this orientation over a head-on sensing approach comes in the data acquisition and analysis portion of the system. It is easier to distinguish slightly varying amounts of light intensity when there is less light than when there is a lot of light. Larger amounts of light will over-saturate the image, making the distinctions between too different intensity reflections less discernible. Analogously, it is easier to weigh the captain of a ship alone than to try to weigh the ship plus captain and subtract the weight of the ship. It is also narrower than the coaxial design, which makes for a much more compact setup. A drawback of this design is that it assumes the vertical scattering will increase as a discernible function of the R_a. Vigilant experimentation was necessary to extract a relationship between the vertical scattering and R_a, and these results are presented on pages 13-14.

Vertical Beam with Pellicle Beamsplitter

In order to address the concerns of working distance and the problems associated with a changing distance, as well as having a compact design, an attractive set-up is a vertical orientation. If the light is collimated, it does not need to be focused at an exact distance from the sample. This set-up uses a 50% transmission pellicle beam splitter oriented at a 45 degree angle from the horizontal, such that half the light is transmitted through to the sample and half is reflected away. Upon reflecting off the sample and hitting the beam splitter again, half the reflected light is again transmitted and reflected. This reflected light, less than 25% of the magnitude of the original light source, less because the sample is not assumed to be a perfect mirror,but is captured by the optical sensor, which sits off to the side. This orientation is the most compact of our choices. It is also the costliest. A high-performing pellicle beam splitter is the most expensive of any of our components by far. It is also a very delicate piece of equipment, it cannot be touched nor have any dust particles on it. This set-up also requires that the light source be especially bright, because it will lose at least 75% of its magnitude from two passes through the beam splitter.

Figure 6: Vertical with Beamsplitter

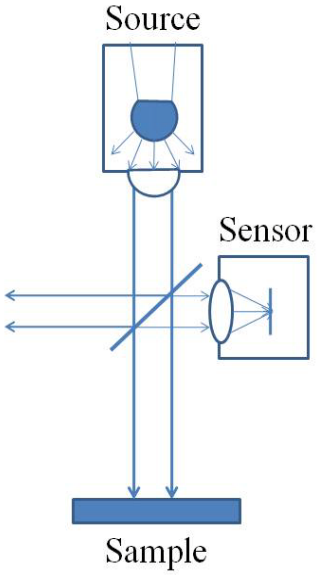

Sub-variations: Light source, sensor, and measurement technique

Within each of these orientations the type of light source and type of optical sensor, and measurement technique are still open to variation. Our original project assumption was that we would be correlating reflected light intensity to a measurement of R_a, however the industry experts at Picometrix introduced the idea of splitting the reflected light and correlating the resulting spectroscopy to a measurement of R_a. In the case of spectroscopy we would use white light as the source, either a CCD or webcam device as the sensor, and any of the three principal orientations. If we chose to measure light intensity, the source could be a collimated LED of any color, a line LED of any color, or even a mercury arc lamp. Given three possible orientations, two possible techniques, four possible source types, and two possible sensors we have forty-eight possible permutations of concept designs.

Given the time constraints of this project we have limited our design space to the measurement of light intensity rather than spectroscopy, and have selected three independent light sources. We designed a set of experiments to enable objective selection of our alpha design among the three orientations, three light sources, and two possible sensors. The following section details our experimental procedure and results.

EXPERIMENTATION

Since the quality of our device is dependent upon the performance of its components, we needed to test the basic performance of the components at accomplishing their fundamental task: creating and detecting differentiation in the images from different surfaces.

Experimental Procedure

We tested the following equipment:

Sources:

Purple LED (67-2064-ND): This source produces 2200 millicandela (mcd) at an operating current of 30mA.

Blue LED (475-2584-1-ND): This source is about ten times brighter than the purple one, producing 20,100 mcd at an operating current of 2A.

White line light: This source is owned by our customer. We do not have much information about the specifications of this source, but it has the advantage of an integrated intensity regulator.

Sensor:

Microsoft LiveCam VX3000 Webcam: 8 bit sensor with a 640 x 480 resolution and a 55° viewing angle.

Figure 8: Experimental Setup

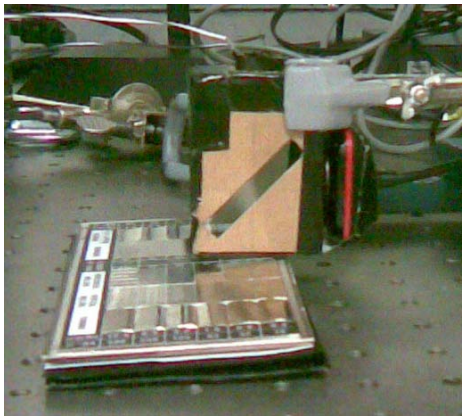

As mentioned previously, our design ideas also incorporated a CCD device. We hoped to test the CCD before this design review, but there were some setbacks. We have a CCD sensor to experiment with, but we were unable to integrate the CCD hardware with our National Instruments Vision Assistant interface. For this reason, we have 9 total sets of data to report (each of the 3 sources in each of the 3 orientations). Each set is composed of 6 reflection images from 6 reference panels of known R_a (0.05µm, 0.1 µm, 0.2 µm, 0.4 µm, 0.8 µm and 1.6 µm) along with average intensity readings for each image.

Aside from the equipment described above, we used some auxiliary components for some of the design set ups. For the vertical design, we used an 80% transmission beam splitter mounted to a simple clamp. For the blue LED light source, we manufactured a fixture made out of Delran to couple the LED with the 7mm collimating lens. The collimating lens did not concentrate the light as much as we had hoped, but it did produce a smaller beam than just the LED alone (size dependent on distance from source). For the purple LED, however, additional collimation was not necessary because the light was already directed and concentrated.

As we assembled each experimental orientation, we were careful to maintain a consistent operating environment for each trial. However, the stands and clamps that we utilized were not designed to record exact angles or distances. Thus, our positioning was somewhat approximate, though completely adequate for this stage of the design process. For each data set, we placed the components in fixtures and oriented the camera so that it delivered a quality image to the computer. Then, we simply captured an image for each standard roughness patch. Finally, we manually selected an area of interest in the Vision Assistant and received an average intensity reading. This average intensity was calculated from a color image, so Vision Assistant reported the results as separate intensities of red, green and blue light. In order to convert these three values into one grayscale value, we conducted some research and found the following industry utilized method for doing this type of conversion [17]:

$$I = 0.299R + 0.587G + 0.114B \qquad \text{[Eq. 1]}$$

Where *I* is the grayscale intensity, *R* is the red intensity, *G* is the green intensity and *B* is the blue intensity. Going forward, we will utilize methods already embedded in Matlab and LabVIEW to convert the image into a grayscale image.

Experimental Results

There are two important aspects derived directly from this experimentation. There are the qualitative visual cues that we got from reviewing at the pictures and the quantitative intensity data using computer software. Figure 7 shows an example of a set of images from the vertical orientation using the purple LED. The round reflections at the top of the images are direct reflections of the source, and the lines of light directly below it are reflected off the test surface. As expected, increasing roughness yields decreasing intensity of the reflection, because the light rays scatter away from the direct path of the beam.

Figure 8: A sample set of images from our data for the vertical set up. As expected, the light intensity decreases with increasing surface roughness.

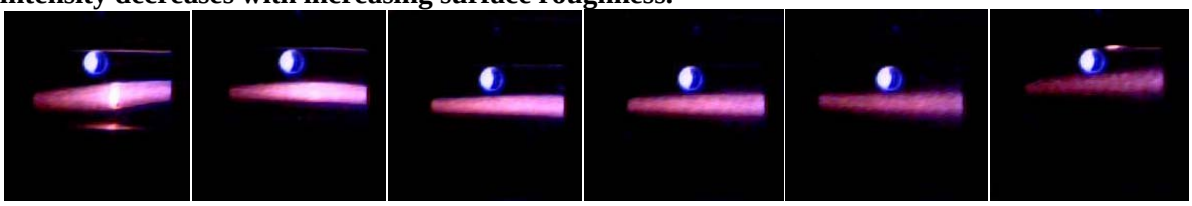

R_a = 0.05µm | 0.1 µm | 0.2 µm | 0.4 µm | 0.8 µm | 1.6 µm

After processing these images, we found the numerical grayscale intensity values using Equation 1.

Experimental Conclusions

The calculated results can be seen in Figure 8. The regression lines shown were added primarily as a visual aid to indicate a trend rather than denote a strict mathematical relation. The data on the following page illustrates some interesting relationships. As we hypothesized, the reflection intensity decreases with increasing roughness for the on-axis and the vertical orientations. For the off-axis, the sensor is placed to capture scatter so the intensity increases with increasing roughness.

The first feature of these relationships that would indicate a good design is the large difference between output intensity values. This creates differentiation that will help when our software assigns an unknown roughness to calibrated intensity values.

Secondly, it is imperative that the curve be monotonic. This is important because the device will need to reverse this curve to calculate an R_a from an intensity. If the curve is not monotonic in R_a, then it will not be a function of intensity. This could result in multiple corresponding R_a values for one intensity reading.

Figure 9: Plots of Brightness Measurements at different orientations

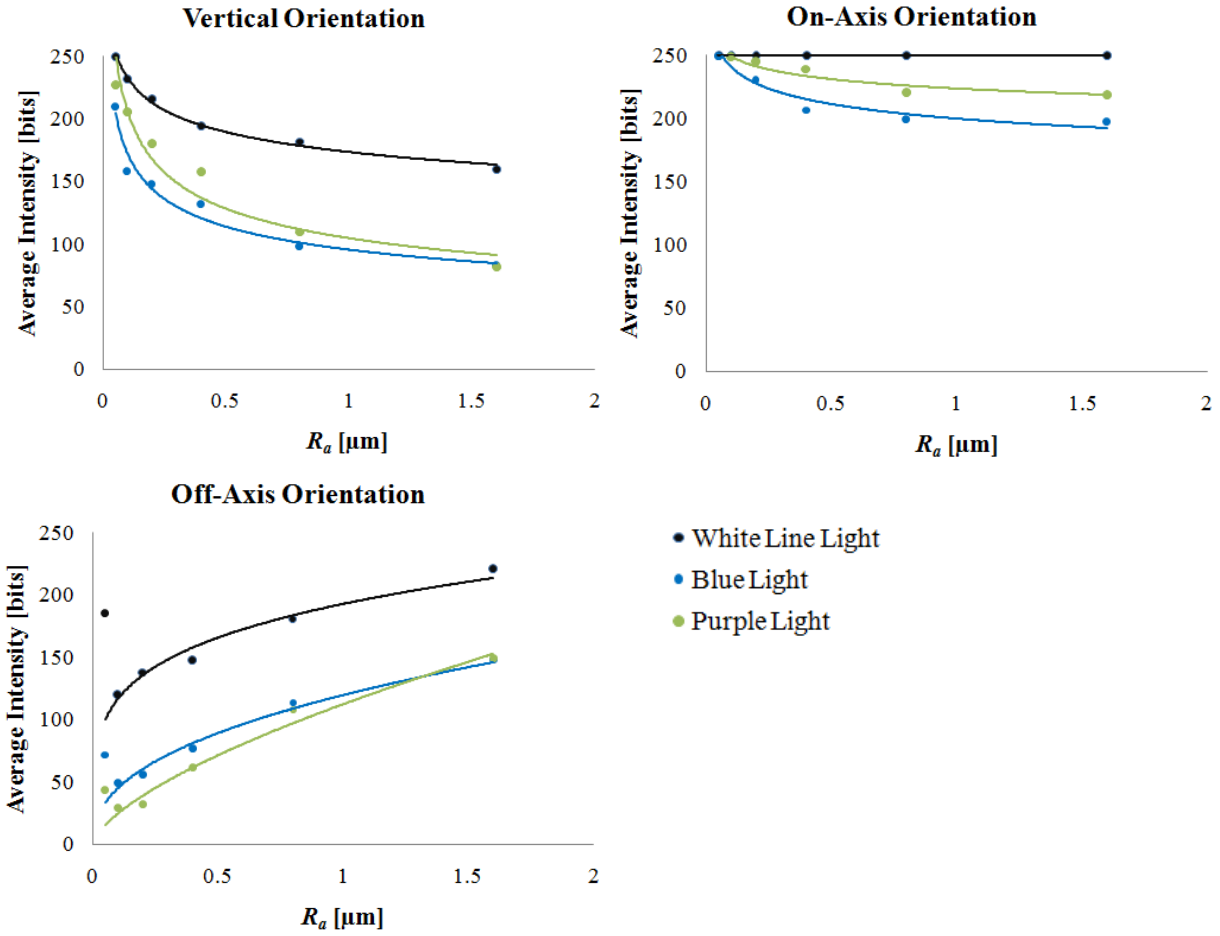

From the above graphs, one can see that from preliminary experimentation the vertical orientation fits those requirements the best. With the on-axis orientation, the webcam was saturating with brightness too easily, which resulted in too little differentiation between each image. We realize that the saturation was a result of experimental setup rather than failure in orientation. Further experimentation is discuss in the Specific Challenges section. With the off-axis orientation, we consistently measured a higher intensity for the smoothest surface followed by the lowest intensity reading on the second smoothest. We attempted to eliminate possible causes such as reflections from the table surface, but this was a recurring issue. There is thus an outlying point at the lowest R_a for each set of data from the off-axis orientation. This outlier was not considered in the fitting of curves to the data.

Experimental Challenges

The procedure for experimentation was a challenge to standardize. It is best that all device and software settings be consistent throughout experimentation. The webcam we used was not designed for such consistency. It was preprogrammed with a wide range of color, contrast, and exposure features. Many of these were set to auto-adjust, which posed a problem when we dealt with low lighting levels. When we attempted to measure small amounts of scatter off a smooth surface, the exposure of the camera increased automatically, skewing our intensity measurement results. We had to change the default settings to obtain a consistent exposure, color, and contrast.

Figure 10: Possible areas of interest

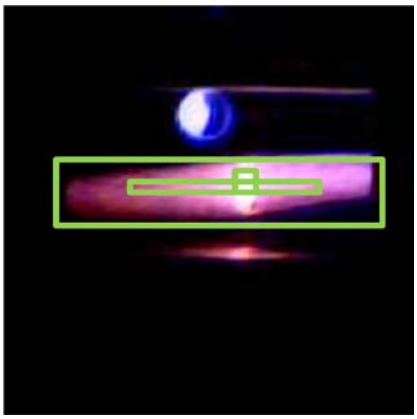

Another aspect that needs to be standardized is the selection of a specific area of interest from the camera image. The viewing angle of the camera encompasses more area than just the light, and for measuring intensity, we want our software to analyze only the portion of the area that includes that light. It is imperative to our success that the image processing algorithm select an optimal area to analyze, since this can drastically alter results. Figure 10 shows an example of an image with some examples of different areas that a user may choose to analyze. In our approach, we thought it was better to select an area that encompasses as much range as possible without getting any of the dark parts. Including a very dark section could potentially yield misleading results, since the amount would be inconsistent for each image.

One challenge that manifested itself primarily in the on-axis design was the saturation of brightness readings on the webcam. This webcam is capable of 256 bit configurations that carry intensity data (8 bits that be either a 0 or a 1). Unfortunately, it was not difficult to make the camera read 'completely bright' and it happened for many of our experiments, even though we were running the white light and the LEDs on minimum intensity. Because of this, we had to minimize the amount of light we were throwing at the surface, which included shielding ambient light. If we can eliminate this problem by using a different source such as the CCD or a different setting, the on-axis design may seem more attractive and ambient light may not be such an issue. However, with our current setup webcam, this is an issue we must keep at the top of our minds.

Finally, it will be a challenge to create the software that will automate the image analysis process, since we are still working on gathering the expertise to do so. This software must have a simple user interface that displays the roughness when the user simply clicks an icon.

CONCEPT SELECTION

After generating an extensive pool of concepts and acquiring experimental data on a more selective group, we developed an objective method of evaluation. This section outlines the method used to effectively assess and score each concept or component of our device. It also provides a brief look at some of the reasoning behind our rankings from the evaluation matrix.

Evaluation Matrix

Our method of evaluation needed to take into account the experimental results and assess other important aspects of the concepts not tested during experimentation. In addition, the evaluation method needed to assess each concept or component fulfilling each sub-function of our device. We developed an evaluation matrix that accomplishes everything mentioned above and assigns a discrete score to each of the possible choices for each sub function. These scores incorporate all of the customer requirements previously outlined in this report, as well as each requirement's relative importance. In order to accomplish this in an organized and efficient manner, we performed research on current methods of engineering design evaluation. We chose to adopt a Borda count election method [18]. In this method, voters rank potential choices, or concepts, for each design criteria, or customer requirement, and the Borda count determines the optimal choice by taking into account the ranks and each relative requirement importance. The completed evaluation matrix can be seen in Table 3 below.

Table 3: Evaluation matrix utilizing Borda count election method used during concept selection.

Customer Needs	Importance	Principal Orientations			Light Sources		
		Vertical	***Off-Axis***	***On-Axis***	***White Line Light***	***Purple LED***	***Blue LED***
Safe for User and Environment	5	2	1	3	2	3	1
Minimized Invasiveness	5	3	2	1	0	0	0
Capable of Discerning between Specified R_a's	5	3	2	1	1	3	2
Capable of Measuring a sample of area 200 mm^2	5	3	2	1	1	3	2
Easily Operable User Interface	4	0	0	0	0	0	0
Low Cost of Implementation	4	1	3	2	1	3	2
Repeatable	4	2	1	3	3	1	2
Completes Measurements Quickly	4	0	0	0	0	0	0
Durable	3	1	3	2	3	1	2
Easily Movable / Portable	3	3	2	1	1	2	3
Aesthetics	1	3	2	1	0	0	0
Total		**82**	**68**	**60**	**48**	**70**	**56**

Evaluation Matrix Justification

The results from our evaluation matrix can be seen in Table 3 above. In the section below, we will discuss in detail some of the thought and reasoning behind the more important rankings.

The rankings for the capability of discerning between specified R_a's were based almost completely off of our experimental results. As discussed earlier in the Experimental Conclusions section, the vertical orientation seemed to eliminate the problem of brightness saturation and the irregular light intensity at a low R_a associated with the other two orientations. In most cases, the purple LED seemed to produce larger differences in light intensity for varying R_a's. From these reasons, we ranked our vertical orientation and purple LED light source highest pertaining to the capability of discerning between specified R_a's.

Although the safety of our device might not seem like an obvious issue, there are some potential dangers and we took these issues very seriously. The major safety concern for a potential user of our device, or any person in the immediate vicinity, is the high intensity light created by the light source. Even during experimentation, it was evident that our potential light sources created light intensity large enough to be hazardous to the human eye. In our vertical and off-axis orientations, a large portion of the light produced is reflected to areas within the device other than the sensor location. In order to prevent this light from interfering with the targeted light being measured, a potential solution was to allow the light to exit our device through some sort of window or opening. In this case, this light could be a potential hazard to the user of the device. In our on-axis orientation, the majority of the light is reflected toward the sensor and there is no need to allow the light to exit our device. From this reasoning, we concluded that the safest orientation would be that of the on-axis. Also, the 2A operating current of the blue LED is a safety concern.

Another major criterion for our device is a low cost of implementation. The vertical orientation setup utilizes a beamsplitter, or pellicle mirror, to split the beam of light in to two directions. This component tends to be very expensive ($150) and would increase the cost of our overall device. The other two orientations do not use this component. In the on-axis orientation, the sensor needs to be positioned to be on-axis with the path of reflected light off of the sample surface. In the off-axis orientation, the sensor is positioned vertically above the sample surface, not nearly as far from the light source. For this reason, we predict that the housing for our device would need to be slightly larger for the on-axis orientation than that of the off-axis (by a couple of centimeters). A larger housing would require more material and result in a slightly larger cost. For these reasons, we ranked our off-axis orientation the highest and our vertical orientation the lowest with respect to the cost of implementation criterion.

ALPHA DESIGN

As can be seen in our evaluation matrix in Table 3, there is an optimal choice for both principal orientation and light source determined by the greatest total score. Our alpha design incorporates these optimal selections into a complete device design. As previously mentioned in this report, we were unable to experiment with our alternative sensor option, a CCD. We do plan to experiment with this option in the future, but for now, our sensor selection will be a standard webcam. This selection is subject to change pending further experimental results. In the remainder of this section, we will further detail our alpha design and briefly discuss some of our major concerns with it.

Figure 11: Alpha Design CAD Drawing

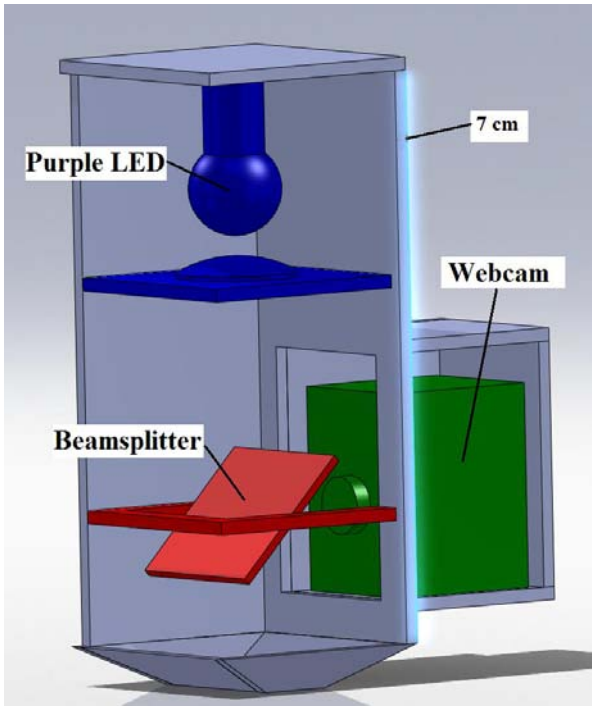

CAD Drawing

A computer aided design (CAD) drawing of our proposed alpha design incorporating the webcam, purple LED and vertical light-sensor orientation was created using SolidWorks 2009 (Refer to Appendix C for more detailed drawings and dimensions). A screenshot of this image can be seen in Figure 9. Although the optimal selections for device components have been tentatively made, the specific model types within these broader categories is not yet know. For instance, although we may have chosen a webcam as our current sensor, the specific webcam model type is unknown. For this reason, the labeled images representing the components are simple, rough drawings with sizes that we feel are accurately comparable to potential model types. The positioning of the elements shown in the CAD drawing is also consistent with our experimental setup. For this reason, we strongly believe that the setup shown in Figure 9 is realistic and fully feasible. As seen in the figure, the overall height of the model is just over 7 cm, and the dimensions for the rest of the model can be understood relative to this.

Our primary concern is the tradeoff between cost and size of our alpha design. The alpha design has the smallest overall size, but also results in the greatest overall cost of implementation, due to its use of a beamsplitter. This component can cost in the range of $200 - $1,000. The minimized size of the alpha design positively correlates with many of the important design criteria such as easy mobility and operability. This tradeoff is a very important issue and one that we will need to further discuss with our customer in order to gain better insight.

A predicted positive outcome of our alpha design is its versatility in working distance. By utilizing the vertical light-sensor orientation, we suspect that a variation in working distance will have a minimal effect on its functionality. In the other two orientations the amount of light being captured by the sensor is directly dependent on the point of light reflection off of the sample surface. The point of reflection is directly related to the working distance. Therefore, working distance directly affects the ability of the sensor to capture light and discern R_a within a reasonable range. The amount of light captured by the sensor in the vertical orientation is not affected by the working distance, because there is no angle of incidence. We plan to do extensive experimentation in the near future to prove or disprove this prediction.

PARAMETER ANALYSIS AND FURTHER EXPERIMENTATION

Image Analysis Algorithm

In order for our experimental data to be viable, the image analysis had to be standardized. As of Design Review 2, our experimental results had been based on analysis of arbitrary areas manually selected from each acquired image. Although we attempted to consistently select the same area each time, we could never trust our results to be entirely consistent unless the process was automated. Thus we formulated several algorithms in Matlab that would analyze the images in different ways, and we compared the results of each one.

Fixed Area Averaging

The first—and simplest—method we tried was to pick the exact same area of pixels to analyze in every image. This was done by first turning the .jpg image into a grayscale array of pixel intensities and then defining specific starting and ending rows and columns as the border of our area of interest. Then we averaged the values of all the intensities within that specific area. This is outlined by the chart in Figure 12. We tested this analysis method with both an area that encompasses the entire patch of light and an area that encompasses just a portion of the light (Figure 13). The drawback of this analysis method is that it does not take into account any slight movements or variation in the location of the light, and the results will thus be skewed if the area of interest is very small and specific and ends up off center.

Figure 12: Method of averaging over a fixed area

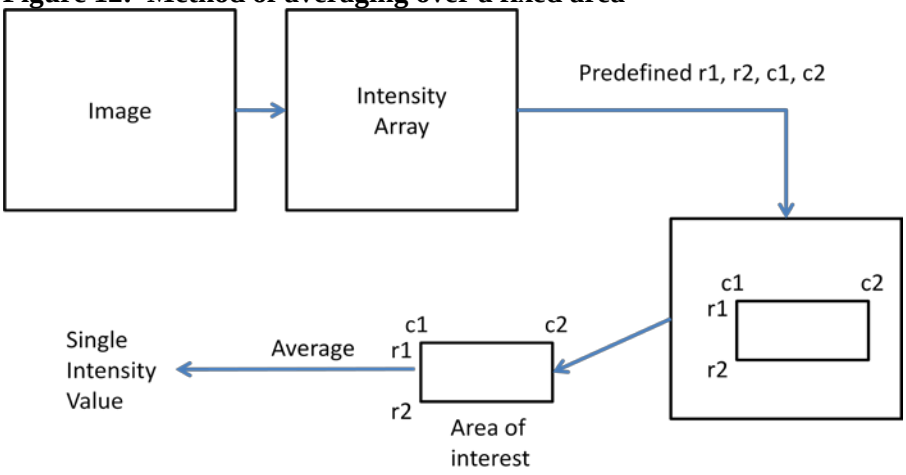

Figure 13: Sampled areas of interest chosen to test algorithm

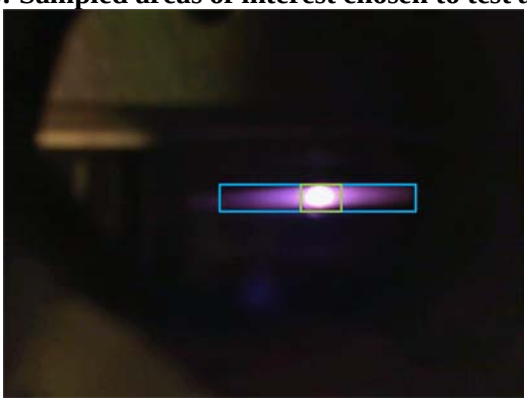

Area Selection Based on Centroid

In order to negate the effects of a possibly shifting light patch, we wanted an algorithm whose area selection was always based on the exact location of the light. This led us to devise a formula that would find the "centroid" of the light intensity, which we assumed would be at the physical center of the light in the image. The formula output the coordinates of this specific point within the image array, and then a constant rectangular area would be defined around that central point. The intensity values within this new constant area were then averaged. This is outlined in Figure 14.

Figure 14: Method of averaging in an area around a centroid

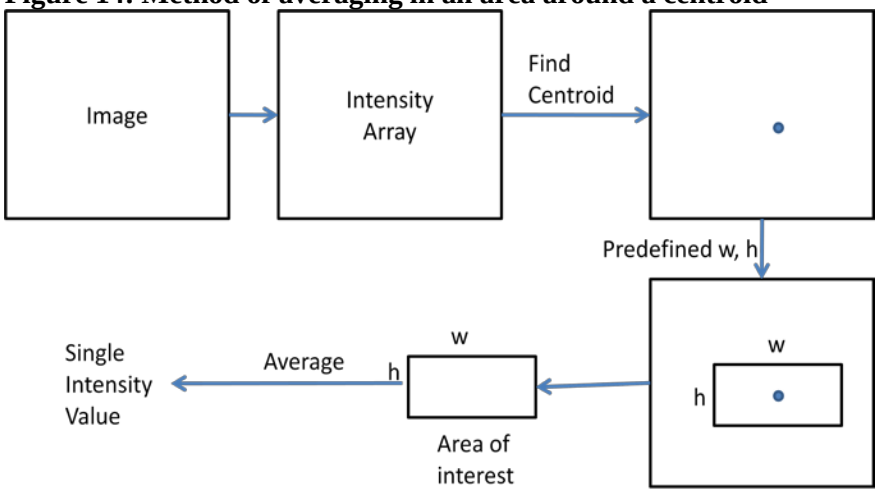

Thresholding and Averaging

Another form of area selection that was considered was based on a threshold argument. It was hypothesized that the amount of pixels above a specific intensity would follow some sort of trend as the surface roughness changed. This algorithm took an image array and disregarded all pixels whose value was below a certain amount, e.g. 82. We would end up with an area of somewhat irregular size as in Figure 15. We then averaged these remaining pixel intensity values. We tested this algorithm at threshold values of 82 (the maximum intensity of light from the roughest sample) and 130. This algorithm is outlined in Figure 16.

Figure 15: Example of an area found from thresholding

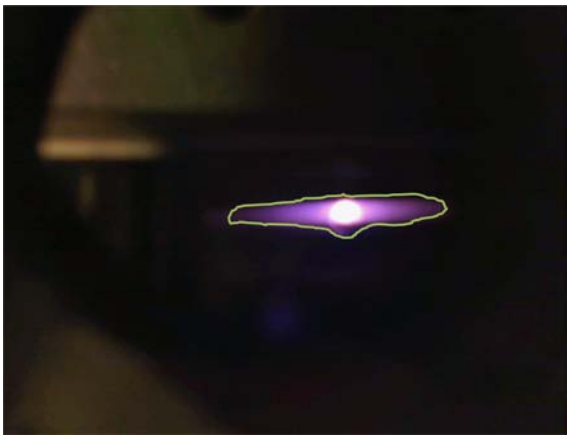

Figure 16: Method of Thresholding

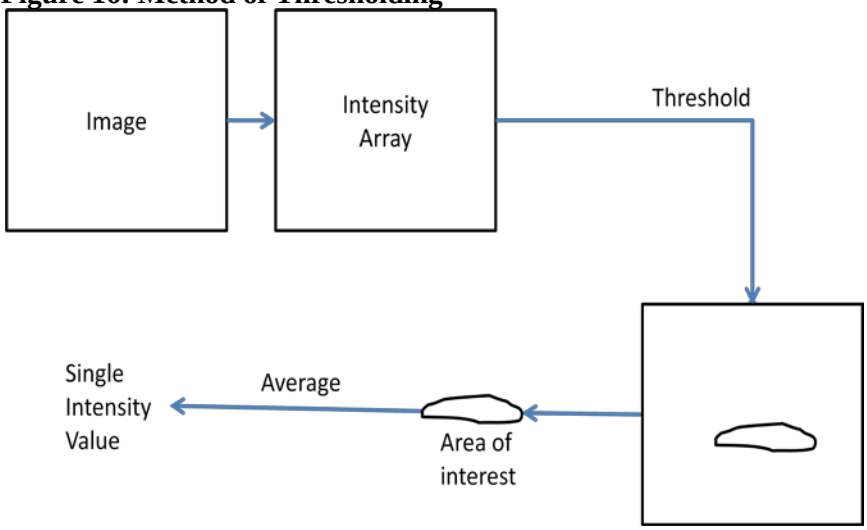

Preliminary Results

After taking five sets of images at each R_a value, we ran each image through each algorithm and received the following results in Figure 17. The fixed area averaging yielded too much inconsistency per measurement with a small area, as shown by the error bars, and almost no differentiation per measurement with a larger area. The threshold averaging yielded a smooth looking curve with little inconsistency per measurement for a threshold value of 82. However, there was not much differentiation between successive points. The centroid method followed a smooth curve, had little inconsistency and large differentiation between each value. Thus the centroid argument became our algorithm of choice.

Figure 17: Experimental results for 5 data sets analyzed with different algorithms.

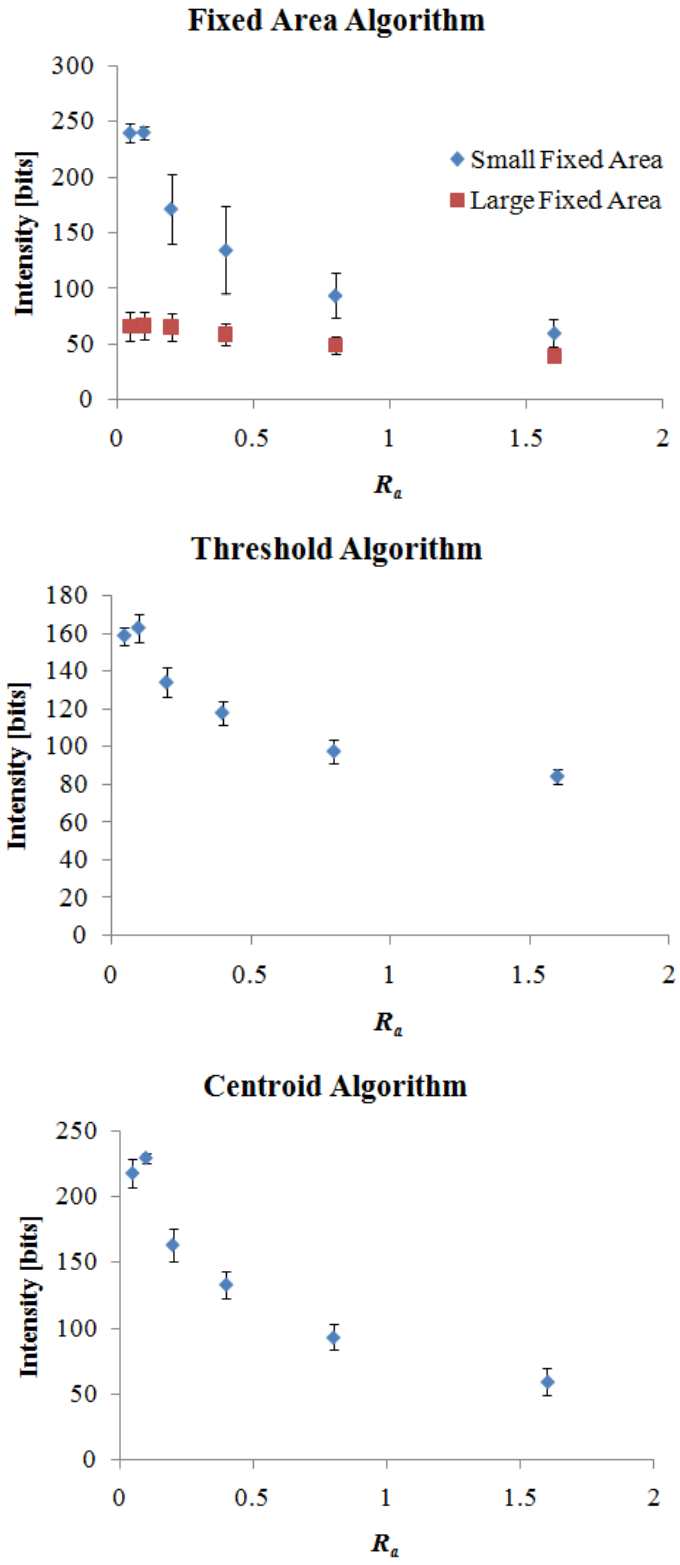

Shape Sensitive Algorithm

In all our results, averaging was incapable of properly discerning the two smoothest surfaces, whose reflected light areas were of comparable brightness. This required another algorithm to be formulated. We noticed that for every set of data, the brightest, most saturated light in each image followed a shape-changing trend from the smoothest to the second smoothest surfaces. The light reflected off the smoothest surface was very circular, and the light from the second smoothest surface was more elliptical, as shown in Figure 18. Thus we created an algorithm that compared the aspect ratio of the brightest light portions of the images. In other words, we thresholded the area above values of 240 and compared the ratio of the height to width of the areas in each image. As expected, the smoothest area yielded a height to width ratio closer to 1 than did the second smoothest area, and there was a large enough difference between the two values to account for any variation in area size as shown in the plot in Figure 19.

Figure 18: Images from 0.05 µm (left) and 0.1 µm (right). Note the more circular saturated area in the 0.05 µm image

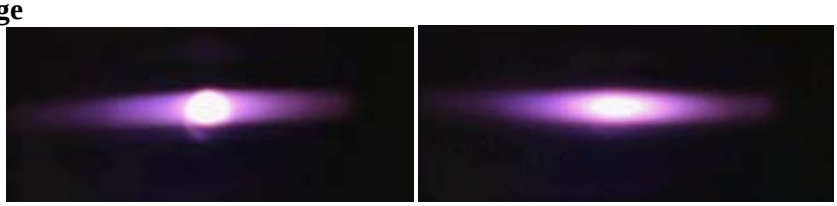

Figure 19: Experimental results for the shape algorithm showing a distinct difference between R_a's of 0.05 µm and 0.1 µm.

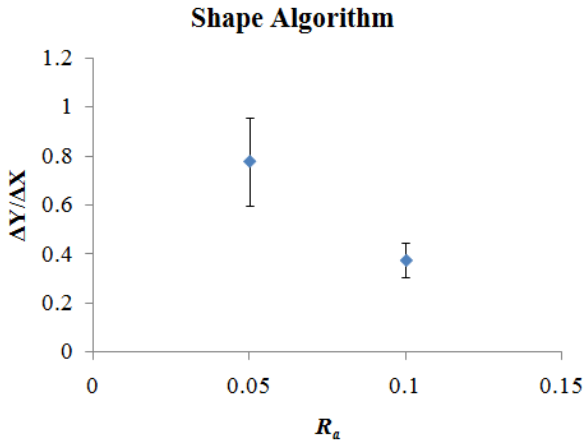

Final Measurement Algorithm

Ultimately, the method used to analyze the images and output the most accurate R_a values used a combination of all the above methods. As outlined in the flowchart, the algorithm turns the raw image to grey scale and makes it an array of intensity values. It then looks at a large predefined area within the image. Within that area, it finds the centroid coordinates of the light and from that point it defines a smaller area centered at the centroid. The intensity values within this area are then averaged. If the average intensity is below a specific value, it is correlated to a specific R_a, chosen by bins defined by the errors from our experiments. If the intensity is above a specific value, the shape algorithm takes effect, and the aspect ratios are correlated to an R_a of 0.05 or 0.1. See the flow chart in Figure 20.

Figure 20: Final measurement algorithm, combining multiple methods of analysis

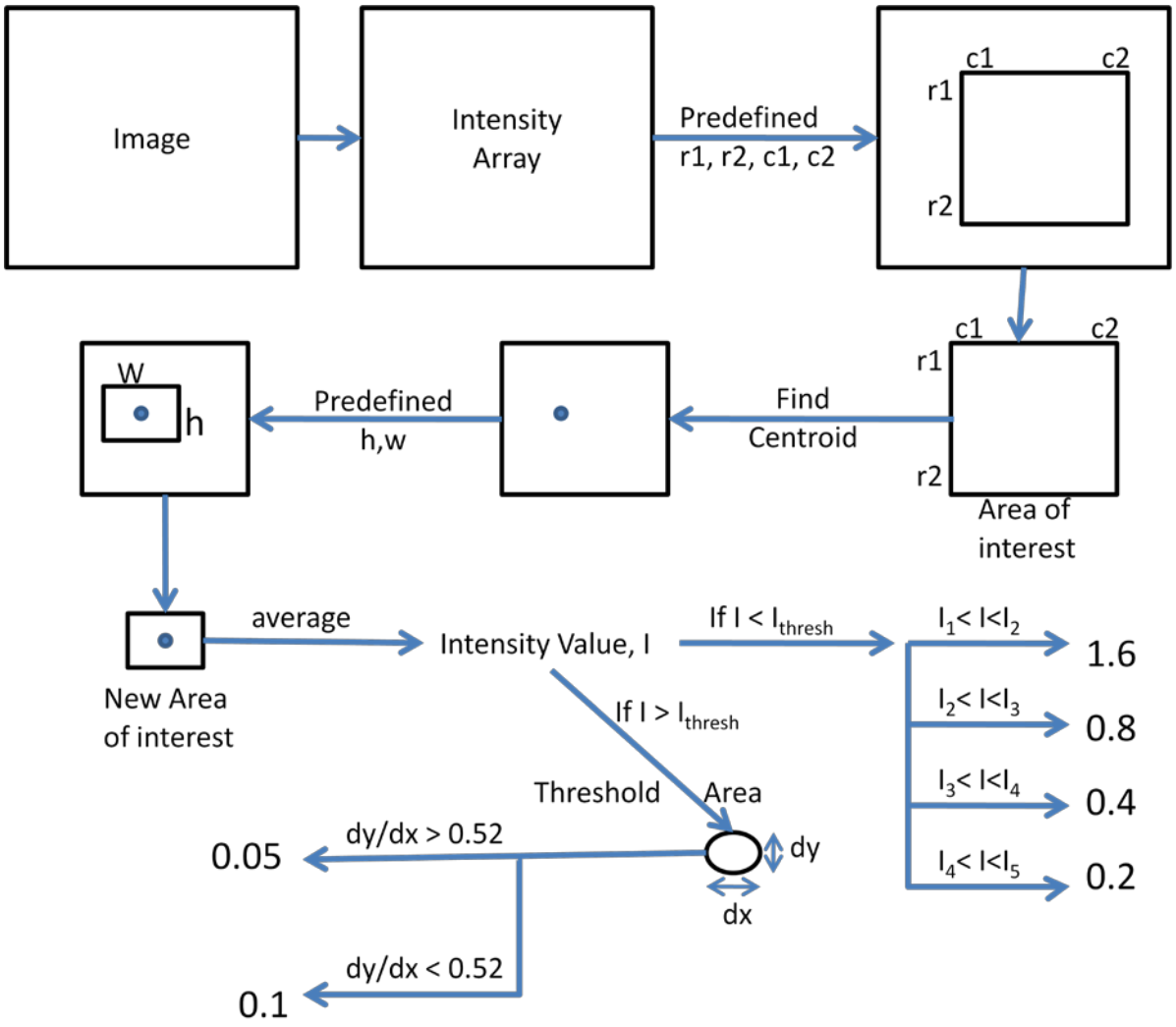

Vertical Misalignment

Earlier, we had hypothesized that our vertical design would be less susceptible to changes in working distance. We performed further experimentation to validate this claim. We excluded the off-axis design due to the outliers in the data that we were unable to remove. Thus, we tested both the on-axis and the vertical design for changes in working distance from 0 mm to 8 mm. All images were taken at a standard roughness of 0.2 R_a and analyzed using the 'centroid' scheme. Figure 21 shows the results from this test.

Figure 21 indicates that the vertical design is indeed more capable of attaining consistent readings for different working distances. There were smaller percent shifts in vertical readings than that of on-axis readings. Also, on the on-axis setup, we placed the light source and camera such that they would be aligned halfway through our test (~3.5 mm height). The readings were somewhat consistent before this point and after this point. However, there was a big shift between 3 mm and 4 mm. This is due to the sudden misalignment of the source with respect to the sensor. Since this design operates with the source and sensor aligned, this data would indicate that a vertical shift of the surface of only 0.5 mm would have a significant effect on our reading. For this reason, we concluded that small changes in working distance would indeed be a concern with the on-axis design.

Figure 21: Results for vertical displacement tests for the on-axis and vertical orientations at 0.2 R_a.

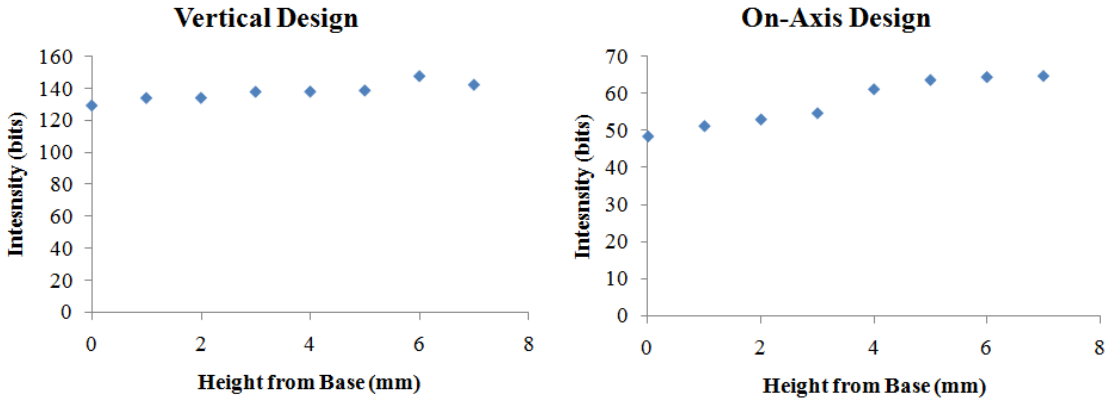

Angular Misalignment

Another important type of surface variation is angular misalignment. We considered two different angles that could be misaligned, and we called them the "long" angle and the "short" angle after the length of the pad that we were rotating. Figure 22 illustrates which rotation is referred by what name.

We ran the centroid algorithm on each R_a value and the shape algorithm for 0.05 and 0.1 R_a for long and short rotations between 0° and 4°. The results can be seen in Figure 23.

Figure 22: Angular misalignment experimental setup showing long and short axis rotation.

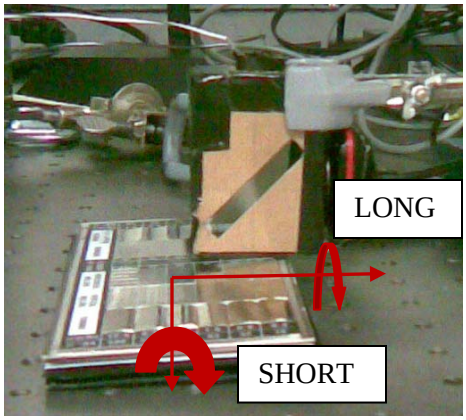

Figure 23: Results for variation of surface angle experiments.

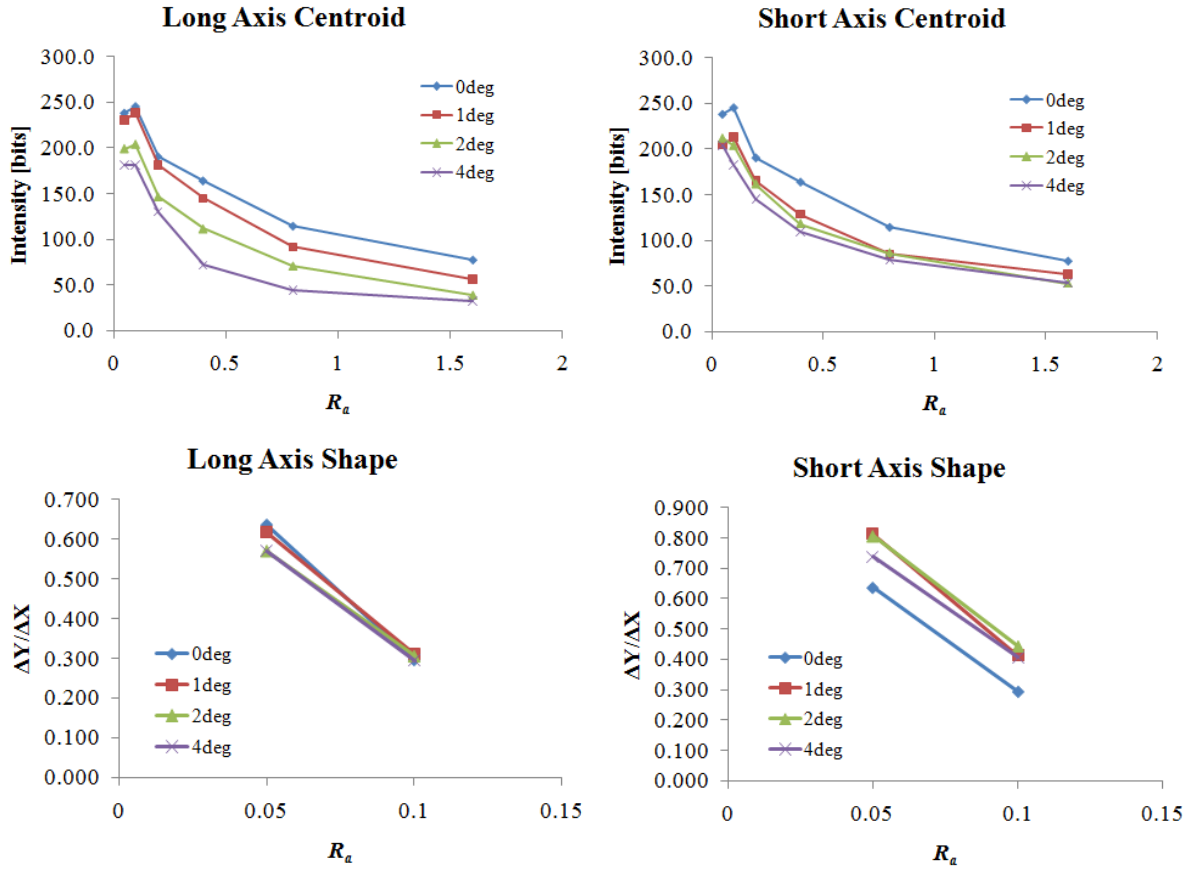

The plots above show that our centroid algorithm is rather sensitive to angular changes. Since this is currently the base algorithm for our device, this is something we must address. The good news is that the overall trend still holds at different angles. This means that our device can be recalibrated to work at different angles. However, if the device has been calibrated to measure at a certain angle and then that angle changes, this data indicates that the readings would no longer be accurate. Moreover, the shape algorithm was surprisingly robust. From the plots above one can see that it would have predicted the proper R_a even without recalibration.

We will attack the issue of the centroid algorithm from two angles. One, we will continue working to make our software less susceptible to shifts in the surface. We will also look into ways of implementing easy calibration procedures and add them if time allows. The other angle of attack is the hardware. We will make a test stand as described in the "Components" section below to ensure that the angle of the device stays constant.

FINAL PROTOTYPE

This section will introduce and give an in-depth description of our final prototype design. It will also provide a description of the components housed inside the device and an assembly and fabrication plan for the prototype.

Description

Our final prototype is made of Acrylonitrile butadiene styrene (ABS) and is approximately 91 mm x 85 mm x 74 mm. It is comprised of three compartments: the main compartment, the top compartment and the side compartment. A computer equipped with our LabVIEW interface must be connected to the web cam housed inside our device during use. Our prototype is fully functional in that it has all of the major capabilities that our final product would have. More specifically, our final prototype has the ability to be positioned over a test surface, capture an image, analyze that image and output a determined R_a value. Figure 24 shows the device both with and without its doors. Note that the computer that the device would be connected to during use is not shown in this figure. Please refer to Appendix F for more detailed drawings. It is also important to note that as part of our final prototype, we will also have a stand on which to mount our device. This stand will hold the device so that the vertical axis of the device is normal to the test surface and will be discussed in further detail in the Components subsection of this section. This stand is not pictured in Figure 24.

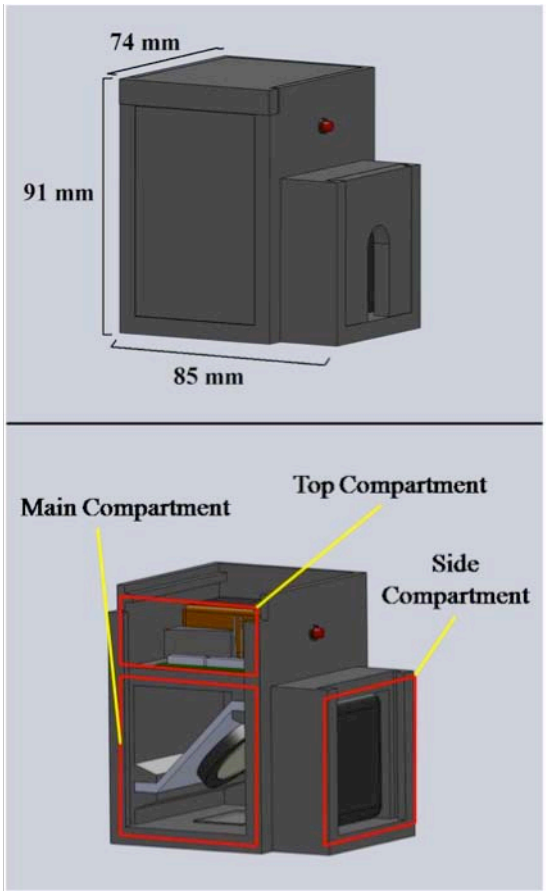

Figure 24: A CAD model of our final prototype both with and without doors.

Modifications from Alpha Design

While performing further experimentation and consulting with our customer, we decided to make some modifications from our previously mentioned Alpha Design.

The most critical modification to our final prototype design from our Alpha design is centered around the doors to the three compartments of our device. There were two doors on the Alpha design that both operated on hinges. The final prototype has three separate doors that all operate on tracks integrated to the main body device. This change allows the user to open the side and top compartments without exposing the main compartment to the ambient environment. This is important because the main compartment houses the pellicle mirror which is extremely sensitive to dust and other ambient elements. These doors were designed so that the friction along the track surfaces suffices to keep them closed during use.

Another modification is that we have eliminated the tapered column leading to the window previously found on the Alpha design. As you can see from Figure 24, the bottom of our device is now flat. This modification essentially brought the potential test surface closer to the pellicle mirror located directly above the window. This modification increases the size of the light reflection in the image as well as makes the device more compact. Our final prototype also uses a 9-volt battery to power the LED. The Alpha design had assumed the LED would use an external power source. This modification allows the device to be more portable. We've also added a transparent protective window to the viewing window on the bottom surface of our device. This window is planned to be made from Plexiglas and will prevent dust and other debris from collecting on the sensitive pellicle mirror. The final prototype also has a removable pellicle holder. This modification allows the pellicle mirror to be easily moved in and out of the device if maintenance or replacement is necessary.

Components

The main body of the final prototype houses eight main components. The top compartment houses the 9-volt battery, circuit board and LED. The LED used in our final prototype is a Luminex 5mm purple LED. In the sidewall of the top compartment, there is a simple push on/off switch that will operate the LED. The switch used in our device is a Mini SPDT 3-Amp Push On/Push Off Switch. The main compartment, found directly beneath the top compartment, houses the pellicle holder, pellicle mirror and protective window. The pellicle holder is a manufactured piece made of ABS, the same material as the main body. The pellicle holder and pellicle mirror are attached to each other with two standard 2-56 screws. When placed in the main body, the pellicle holder holds the pellicle mirror at a 45˚ angle with the horizontal. The pellicle mirror used in our device is an Edmund Optics 1" Diameter 50R/50T Pellicle Beamsplitter. The protective window is also a manufactured component that is made out of Plexiglas. The side compartment houses only the web cam. The specific web cam used in our final prototype is a Microsoft LifeCam VX-5000. Figure 25 below shows a model of the final prototype with the main body shown as transparent so the components are clearly visible.

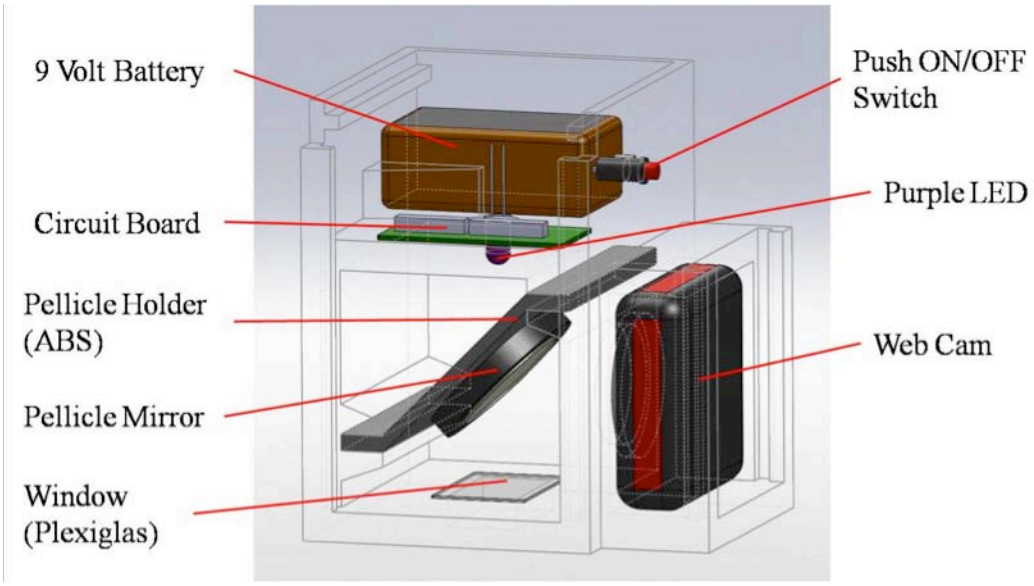

Figure 25: A model of the final prototype showing the eight main components housed in the device.

Fabrication

After we developed our final prototype design, we generated three possible plans to fabricate our device. The three potential fabrication plans were subtractive machining, additive machining and rapid prototyping.

In the subtractive machining plan, we would essentially start out with one solid piece of stock material and subtract, or machine, out blocks of material to form the various cavities. The three compartments described earlier would be machined out most likely using a mill and the various holes would be created using a drill. Although this plan produces a very robust, single-piece main body, the cavities for the three compartments in our design are quite complex and would making milling very difficult.

In the additive machining plan, the main body of the device would be manufactured in pieces and then assembled together with mechanical fixtures or adhesive. The main and top compartments would be manufactured by removing material from a block of stock material using a mill. The side compartment would be manufactured separately in the same manner. These two pieces would then been joined using

mechanical fixtures. This plan again requires difficult milling operations to create the cavities for the compartments as well as adds additional fixture components to the device.

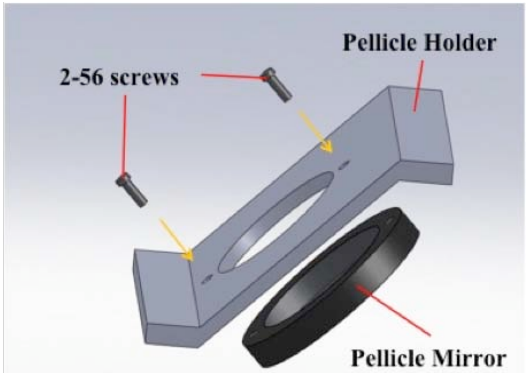

Figure 26: Pellicle assembly showing labeled components.

In the rapid prototyping plan, we would utilize a unique three-dimensional printing service available to us at the University of Michigan to have the entire body of the device made in a single piece of material. The three-dimensional printing service uses a machine called the Dimension FDM Elite to create a layered composite object from a CAD file. The Dimension FDM Elite is capable of producing extremely complex geometries with tolerances as small as 178 μm. In this plan, we would generate a precise CAD model of our prototype and import this file into the Dimension FDM Elite in .STL format. The turnaround time for an object of our size and complexity would be approximately 40 hours. Minor post-process machining such as sanding would then be done to the completed body.

The most important factor in our final choice of a fabrication technique was the accuracy of our manufactured components. The success of our design heavily relies on the precision of the angle at which the pellicle mirror is held. As mentioned earlier, the milling operations required to machine out the cavities for the compartments is quite complex and we did not feel that we would be able to accomplish the accuracy necessary. For this reason, we chose the rapid prototyping technique to manufacture our prototype. The main body, the doors and the pellicle holder will all be manufactured using this method. All of the parts made with this method will be made out of ABS, a rigid, lightweight thermoplastic. As mentioned earlier, this fabrication method builds the parts through an intricate layering process. For this reason, the final parts do have varying directional strength. The material is fairly resistant to forces applied normal to the layering, but could be less resistive when a load is applied parallel to layering. Because our device has no "expected" loads, we do not foresee this being a major problem. This technique allowed us to greatly decrease our estimated manufacturing and assembly time. The total cost of this type of manufacturing, including material, labor and machining costs, will be $170.

Assembly

The assembly of our device is quite simple. As previously mentioned the main body of our device will be manufactured as a single piece and requires no assembly in itself.

The first step will be to attach the pellicle mirror to the manufactured pellicle holder. The pellicle mirror has a hard plastic ring around the mirror that has two tapped holes. The pellicle holder was designed to be manufactured with two through holes positioned to match up with the tapped holes on the mirror. Two standard 2-56 screws will be used to attach these two components. Figure 27 shows a schematic drawing of this assembly.

Next, the circuit board, protective window and on/off switch will be attached to the main body in their respective locations using standard epoxy. It is important to note that the circuit board, consisting of simple wiring and resistors, will be assembled outside of the main body and then epoxied in. The main body has been designed so that the 9-volt battery, purple LED, web cam and pellicle unit (the attached pellicle mirror and holder) can all be press–fitted in to their respective locations. Lastly, the three doors slide in to the main body on integrated tracks. Figure 27 shows the main body after fabrication before assembly and the fully assembled main body.

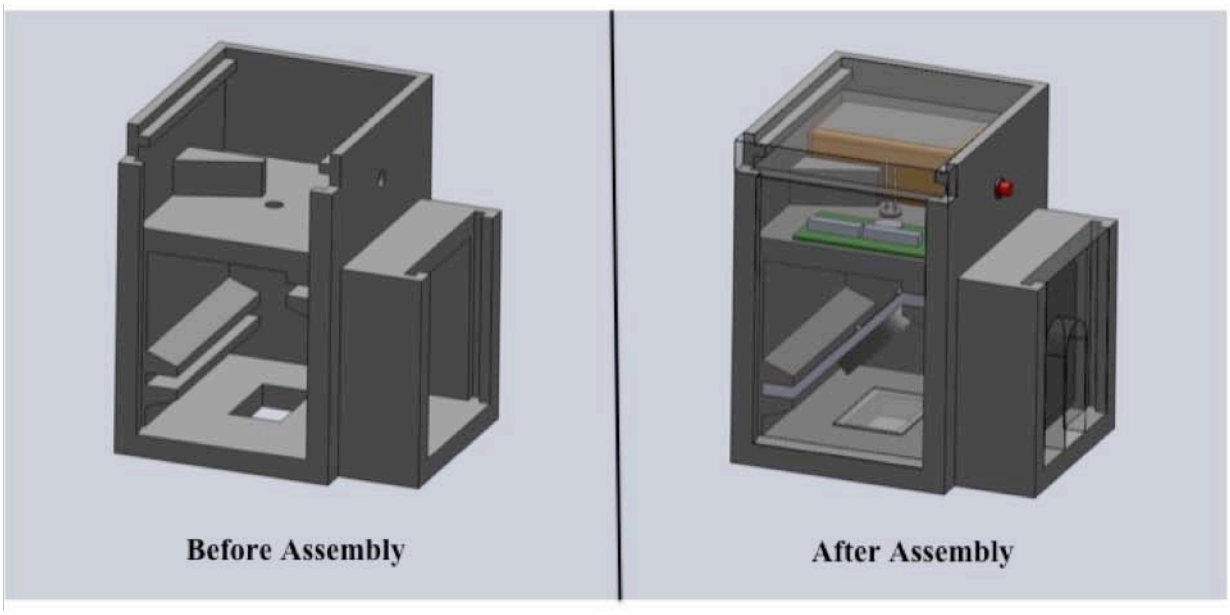

Figure 27: Prototype before and after assembly.

User Interface

The user interface that a potential user would encounter on the computer connected to our prototype was created using LabVIEW. Figure 28 shows a screenshot of the user interface. For our prototype's most basic feature, a potential user only needs to perform three steps. First, the user needs to physically position the device directly above the surface being measured. This can be done by either moving the surface while keeping the device stationary or vice versa depending on the nature of use. After the prototype is positioned correctly, the user uses the "Snap Picture" button on the interface VI to capture an image. In order to ensure that the user captures an image of the desired surface region, there is a "Live Image" window featured on the VI to allow the user to see the potential image to be captured. Lastly, the user uses the "Analyze Image" button on the VI to command the interface to process the image and output a determined R_a value. The VI also offers more complex features that allow the user to alter camera settings, threshold limits and geometric area selection parameters. These options are strictly for calibration purposes and are not needed during standard use.

Figure 28: A screenshot of the LabVIEW user interface encountered during use of the prototype.

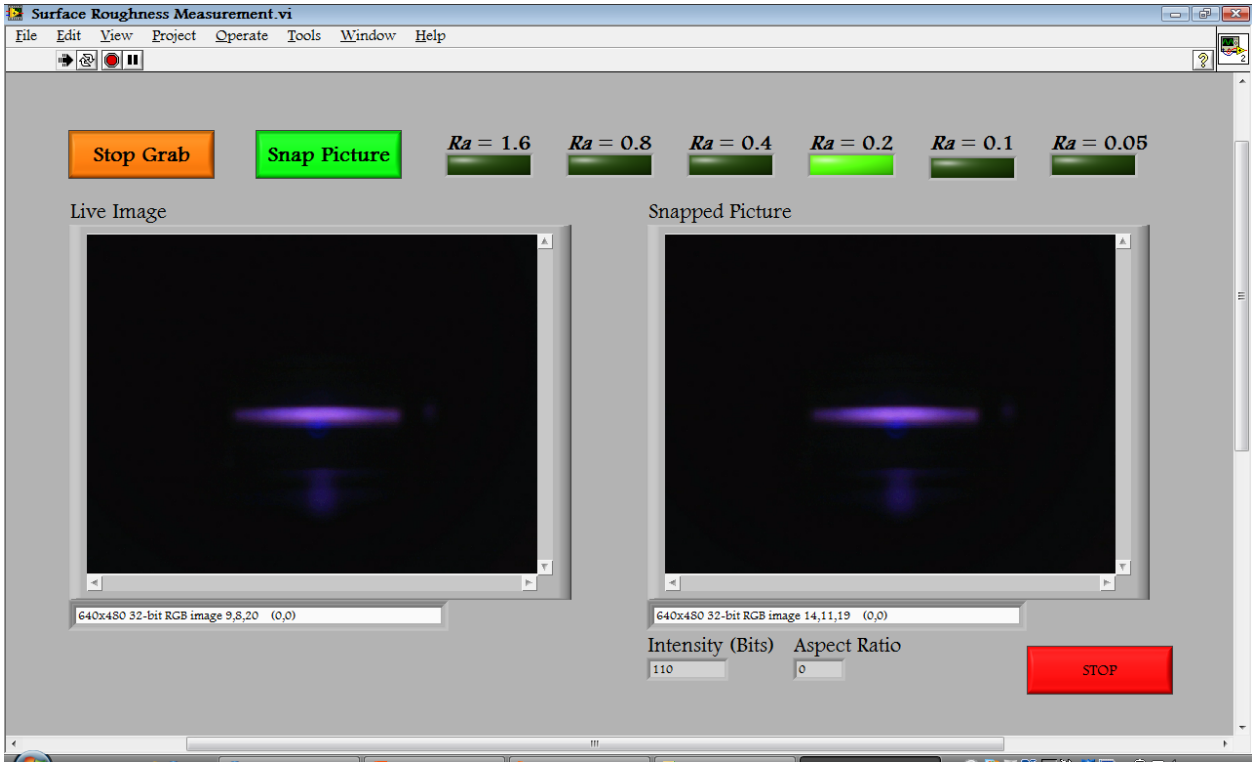

FINAL DESIGN CONSIDERATIONS

This section will outline major differences between our final prototype design and the final, marketable design of our device. These differences arise primarily due to the major differences in expenses and ease of manufacturing between producing a single functioning prototype and mass-producing a marketable product.

Material Selection and Fabrication

For our one of a kind prototype it was rather clear that rapid prototyping was the optimum method of fabrication. With the resources available to us here at the University, we only had two options: a brittle plaster powder ($0.20 per cc) or ABS plastic ($0.40 per cc). We chose the latter for its strength and machining capabilities.

However, when designing a final product intended for market, we had to look much more carefully at potential materials and fabrication methods. The tool that we utilized to do this is CES EduPack 2009. This software is essentially a huge database of materials and manufacturing processes. The user can specify limits for various properties and the software will keep track of the materials that meet the criteria, as well as will show what processes may be performed to the materials. Table 4 shows the limits that we used for our design.

Table 4: CES Parameters for the final design.

Parameter	Minimum	Maximum	Unit
Price	0	1.3	$/lb
Max Service Temperature	120	-	°F
Min Service Temperature	-	50	°F
Electrical Resistivity	1×10^6	-	µohm.cm
Transparency	Opaque		-
Water Resistivity	Excellent		-
CO2 Footprint of Production	0	4	lb/lb
Recyclable	Yes		

From the table one can see that we are concerned with price, durability, optical properties and environmental effects. We want a device that will cost at most a few dollars of material. Also, it must operate in temperatures that will be expected in a typical manufacturing line, so the maximum should be above 120°F and the minimum should be below 50°F. The material should be able to resist water and it should not conduct any electricity from the circuitry in the top compartment. Moreover, we tried to minimize adverse effects on the environment by limiting the carbon footprint of production to a rather low value (4 lb/lb) and by making our product out of a recyclable material. The list of materials that fit these criteria is shown in Figure 29, ranked by price.

Figure 29: All materials fitting our selection criteria

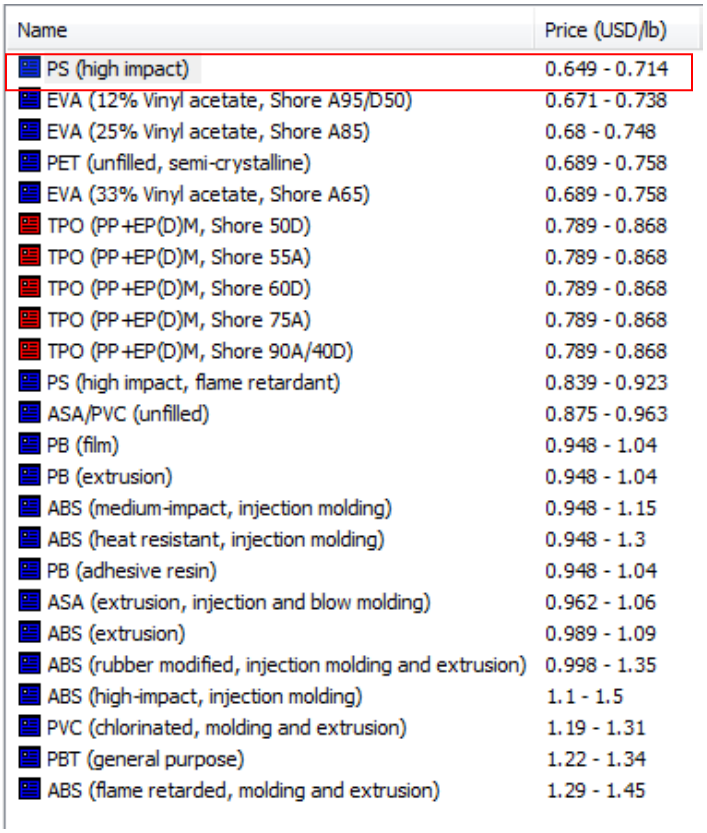

Figure 30: Manufacturing processes for high impact polystyrene.

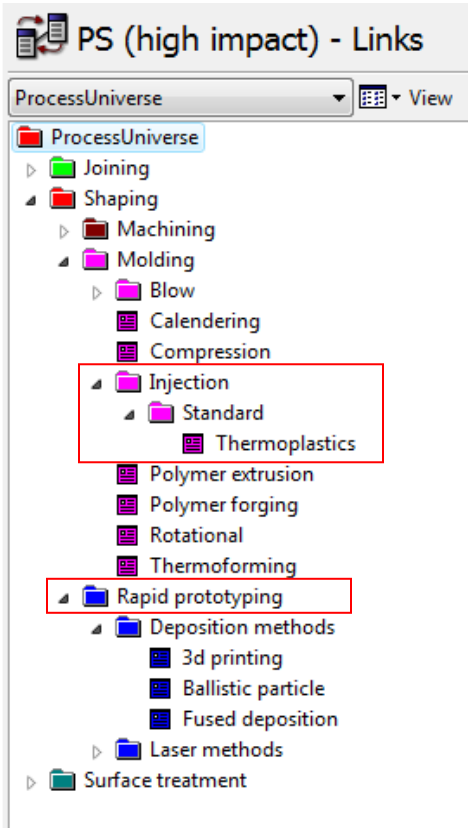

From Figure 29 one can see that the cheapest material that fit our criteria was HIPS, or high impact polystyrene. This is a low density (0.038 lb/in^3) polymer with impact modifiers for greater impact resistance. This material allows our device to be light, cheap, durable and environmentally friendly. In fact, with this material our device would weigh 0.4 lbs (with no components) and would cost $0.28 of material. This material is often used to make toys and household appliances, and it does not deform very easily ($E = 3 \times 10^5$ psi).We feel that this would be the best material to use for the main block and all the doors – every part that is not directly bought as a component. Please refer to Appendix E for more information about this material.

Another great feature of the CES software is that it suggests manufacturing processes that are compatible with materials in its database. The CES process suggestions for HIPS can be seen in Figure 30. Most of the processes shown would not be suitable for our device. All common machining processes (such as milling, turning, drilling, etc) would not be adequate for making our device. These processes would not be able to make such intricate detail on such a small scale while keeping tight tolerances. Thus, we eliminated these processes from our palate. Also, most methods of molding would also not work with our device as it is currently designed. Processes such as blow molding, polymer extrusion, rotational molding, or polymer forging are not able to create very detailed shapes with multiple compartments. We were left with thermoplastic injection molding and rapid prototyping.

The decision between these fabrication methods then comes down to the market size and the amount of fabrication we intend to undertake. Injection molding has very high initial tooling costs (from $3,000 to $90,000 for a mold) but can produce many units very quickly (60 to 3000 per hour) for low additional cost. Rapid prototyping, on the other hand, has low tooling costs ($40 - $90) but these costs are recurrent for every unit. Also, the production rate is only 0.02 – 0.5 units per hour. Thus, for small production sizes, we would rapid prototype our device in polystyrene. However, if we were to sell about 10,000 units or more we would use thermoplastic injection molding for fabrication.

Components

Another major difference between our prototype and the final product is in the individual components inside the device. Some of our components are marketed products designed to be stand-alone devices with unnecessary casing and features. In a mass-production scenario, these parts would be replaced with "bare" components bought in bulk straight from the manufacturer. These modifications would most likely make our complete device cheaper and more compact. These changes, along with some others, are discussed in greater detail below.

As previously mentioned, the sensor used in our device is a Microsoft LifeCam VX-5000. This product is marketed as a web cam mostly intended for users looking for a method of live communication over the Internet. The web cam consists of the camera itself as well as a USB compatible cable to connect to a computer. As one would expect, the camera comes with a protective and aesthetically pleasing casing and loads of user options to alter camera settings. Due to its nature of use, the web cam is also designed to have a very wide viewing angle. These detailed camera-setting options, extraneous casing and wide viewing angle are not at all ideal for our intended use of a sensor. Our ideal sensor would be small, have very basic, if any, camera-setting options, and have a much narrower viewing angle. We foresee the sensor component used in the final product as still having a USB compatible connection to connect to a computer. In order to decrease the viewing angle and also add greater resolution to our sensor, we would mostly likely utilize a lens in conjunction with our sensor. For the resources available to us and the nature of our single prototype, these modifications are not practical. However, in a final product, these changes would increase the quality of our device, decrease the overall cost of our device, and allow our device to be more compact.

Our final prototype uses a standard 9-volt battery to power the LED housed in the top compartment. We chose this component because it best suited our needs and intended purpose for the prototype. The power used for the final product is very dependent on its intended use. The requirements of the power source are very simple and could be met by a multitude of different options. If the final product were meant to be permanently mounted on an assembly line in a factory setting, utilizing an external power source might be the most practical option. If the device is intended to be constantly moved to be used in various locations, a battery powered setup similar to that of our prototype would most likely suffice. As one can see, there are many options for the power source and we feel that our design could be easily catered to meet the needs of almost any specific use.

As previously discussed, our device's accuracy is sensitive to the angle of the test surface relative to the vertical axis of our device. Our device is capable of functioning at angles deviating from the vertical axis being normal to the test surface, but a recalibration procedure would need to be performed. We have integrated features in to our user interface to allow the user the options necessary to manually recalibrate the system, but in a marketable product, this issue would be addressed to a much greater degree. Not only would we include more calibration-related options in the user interface, much of the process would be automated. We would also most likely develop a user manual solely dedicated to recalibrating the device.

VALIDATION TESTING AND RESULTS

In order to complete the design process, we must validate that we have in fact met all of the customer requirements outline on Page 7 of this report. We have stayed within our budget of $400 (see Appendix A for a detailed breakdown of the costs) and our device does not touch the surface that it is measuring (15mm standoff). Table 5 shows other engineering parameters, the target values we had established and the final results.

Table 5: Results of engineering parameters.

Rank	Parameter	Target	Result
1	Optical Sensor Resolution	8-bit	8-bit
2	Standoff	1 - 10 mm	1 - 30 mm
3	Light Wavelength	380-750 nm	480 nm
4	Light Intensity	< 5000 mcd	< 2000 mcd
5	Measurement Time	< 3 sec	< 1 sec
6	Steps in Operation	1 step	1 step
7	Weight	< 1 kg	< 1 kg
8	Size	< 150x150x400 mm	85x75x90 mm

The table shows that we met or exceeded all of our targets for the engineering parameters. In order to validate the accuracy and repeatability of the device, we performed detailed validation experiments that are outlined in the following section.

Reliability Validation

Each trial, or each measurement, of our device can be interpreted as a Bernoulli trial (it can either succeed and output the proper R_a, or fail and output the wrong R_a). Since each trial has some probability of failing, and this probability is not affected by other trials, we felt that the best statistical test for reliability of our device would be a Binomial Test. For each of the configurations below, we utilized a 95% confidence interval to find the bounds for the probability of proper functionality. For all tests, our device was set to output results according to the thresholds shown in Table 6.

Table 6: Thresholds for the device.

R_a	Intensity (bits)	Aspect Ratio
0.05	>145	> 0.6
0.1	>145	< 0.6
0.2	100 - 145	
0.4	75 - 100	
0.8	45 - 75	
1.6	< 45	

15mm standoff, 0° angle

This was our baseline set of trials. The device is designed to operate at a 15mm distance from the surface of interest and normal to the surface. We performed 120 trials (20 sets of 6 pictures) with this configuration and all of the pictures output the proper results. This yields a confidence interval of 0.97 – 1.0, meaning that we expect the device to work at least 97% of the time.

We also recorded the output intensity and aspect ratio for each of the trials, so that we could get an idea for how robust the device is. Table 7 shows the average intensities, the aspect ratios, and the errors based on the 120 trials. The errors reported are two times the standard deviation between all the trials. The table shows that the errors of the experiments were very small (maximum of 2.45 bits and 0.045 aspect ratio) compared to the gap between the averages (23 bits and 0.484, respectively). This gave us much confidence in the reliability of our device. The next step was performing similar tests with changes in standoff and changes in angle to capture the sensitivity of our device to movement or misalignment.

Table 7: Results for baseline tests at 15mm standoff and 0° angle.

R_a	Average Intensity	Error	Aspect Ratio	Error
0.05	198.10	2.04	0.882	0.045
0.1	181.65	2.45	0.399	0.022
0.2	111.35	1.75		
0.4	87.00	2.05		
0.8	56.45	1.52		
1.6	33.45	1.21		

Changing standoff, 0° angle

The next experiment was to change the standoff by increments of 2mm to test the device sensitivity. This was done using 3 spacers of 2mm each. We set up the device with the usual 15mm standoff with one spacer already placed. Then, we added a spacer to get readings for +2mm and removed the original spacer to get the reading for -2mm standoff.

Figure 31: Standoff misalignment results. The lines shown are the thresholds between the R_a values.

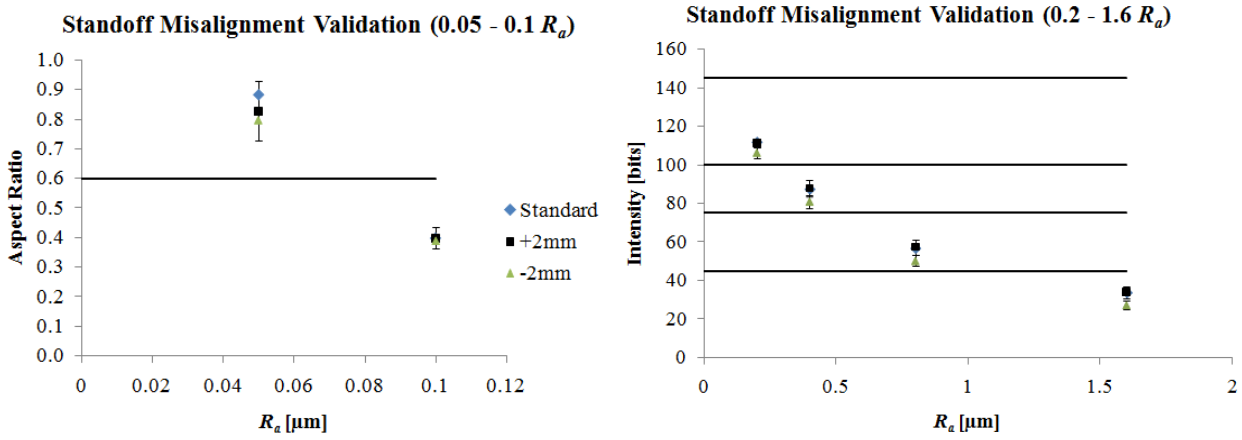

We performed 60 trials for +2mm and 60 trials for -2mm and the device succeeded in getting the proper reading in all trials. This translates to a confidence interval of 0.95 – 1.0, meaning that we expect the device to work at least 95% of the time. The results can be seen in Figure 31.

The lines that are shown are the thresholds between the R_a values, and the errors are two times the standard deviation of the readings. The graphs show that within error all of our readings lie within the proper thresholds. Thus, we are comfortable asserting that our device is capable of operating within 2mm of vertical misalignment without the need for recalibration.

It is also relevant to find the bounds of standoff where the device is operational with recalibration. To perform this test, we started at 1mm of standoff (just barely above the surface) and took 3 sets of 6 readings. We noted that the results were such that a calibration routine could be written to differentiate between the six R_a's reliably. We repeated this process for 5mm, 10mm, 15mm, etc until the algorithm broke down. We found that the algorithm starts to become unreliable over 30mm of standoff. The biggest factor that contributes to this is that the useful part of the image becomes smaller as you increase the standoff. Thus, after a certain point, the algorithm starts to catch some area outside of the light reflection when it averages the intensity. Also, when we increased the standoff we started so see the adjacent surfaces in our images. These can also throw off the measurement by introducing extra reflections in the image. From this, we concluded that the device can operate between 1 and 30 mm of standoff with recalibration.

15mm standoff, changing angle

The final validation experiment was to rotate the long axis of the surface of interest by 2° to simulate angular misalignment. We achieved this by placing spacers on one side of the scratchpad with the proper height to create a 2° angle (the length of the scratchpad can be measured, so this is a simple trigonometry problem).

Figure 32: Angle misalignment results. The lines shown are the thresholds between the R_a values.

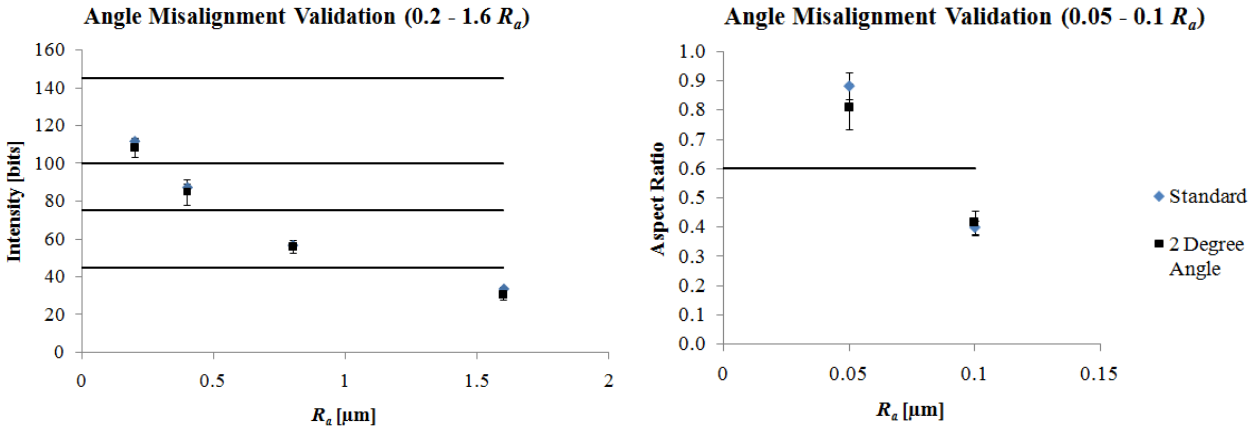

We performed 60 trials with the angled surface and the device succeeded in all 60. This translates to a confidence interval of 0.95 – 1.0, meaning that we expect the device to work at least 95% of the time. The results can be seen in Figure 32. As before, the graphs show that within error all of our readings lie within the proper thresholds. Thus, we are comfortable asserting that our device is capable of operating 2° off of angular alignment without the need for recalibration.

DESIGN CRITIQUE AND RECOMMENDATIONS

We are very proud of our final device and its capabilities. There are many aspects of our device that exceeded our initial expectations and some that we would look to improve upon if given more time. The purpose of this section is to outline these strengths and weaknesses.

Strengths

Our initial project objective was to design and build a test stand to explore using visible light to determine surface roughness. One aspect of our work that we are very proud of are our efforts in taking the initial steps towards making our device a marketable product. Our final device is much more than a test stand. Its small, compact design makes the device easily portable and usable in a variety of practical settings. Our device's design also allows for all major components to be press-fitted into the device, eliminating the need for fasteners with the exception of the two screws fixing the beamsplitter to its removable frame. We feel that this feature makes the assembly process on a mass-production scale much more feasible.

Another feature of our device that we feel is very impressive is its robust functionality and build. We expected our device's function and accuracy to have decreased sensitivity to changes in the home position when compared to that of laser devices, and our validation results confirmed our expectations. As can be seen in our "Validation Testing" section, our device successfully functions with significant changes in working distance and angle without recalibration. By creating the main body of our device from a single piece of material, the build of our device is also very robust. Although the device is not intended to encounter any forces beyond normal "handling" wear, we feel that this increased durability is a strong aspect of our device.

Potential Improvements

One option that we would have explored given more time is the addition of a diffuser to the light source. A diffuser would essentially scatter the light before reaching the test surface, allowing for a more even distribution of light across the region of interest. Our current device utilizes a round LED with no

diffuser, and light distribution on the test surface is therefore a circular pattern. We feel that by adding a diffuser and spreading the light more evenly across the surface, we would be able to simplify our algorithms to be solely based off of light intensity (our current algorithms analyze light intensity and shape). We also feel that this addition would reduce the chance of error in our device caused by a small surface abnormality.

Another aspect of our device that we feel could be improved upon is the resolution of our captured image. Our current sensor setup has a field of view much larger than is needed for our purposes and uses only a small fraction of our sensor's available pixels. With the addition of a lens to our sensor, we would be able to decrease the field of view to an optimal size and drastically increase the resolution of our captured image. Theoretically, an increase in the resolution of our captured image should allow our algorithms to perform a more detailed analysis, and better differentiate between varying values of R_a. Extensive experimentation would have to be done in order to determine what type of lens would produce optimal results for our device.

Finally, our current device requires a manual calibration process each time a change in the standoff of greater than 2mm has been made. In order to improve the user convenience of our device, we would look to expand the functionality of our code and user interface to include an automatic calibration process. The current manual calibration process essentially consist of capturing images of a set of known surface roughness values, analyzing the algorithms' resulting light intensity and shape parameters, and setting the threshold values such that the surfaces with differing roughness can be optimally differentiated. With more time and effort, our existing code could be expanded to automatically determine threshold values from a set of known images.

Suggested Directions

To expand the scope of our project, we have recommendations to our sponsor for future paths to explore. The purpose of this section is to describe these paths and the impact that they could have on our device.

Our current device is meant to be used only on ground, flat surfaces. We believe that a worthwhile endeavor in the future is to explore the possibility of using our device on other types of surfaces. More specifically, our device should be tested on contoured surfaces that have been manufactured in manners other than grinding, such as milling, turning, or reaming. It is possible that our device could work on surfaces such as these, but may need a different set of algorithms to do so. The feasibility of this option could be determined through experimentation. In order for this device to be practical and useful in a real-world setting, its use needs to be extended beyond the realm of flat, grinded surfaces. Exploring the path described above would be the first step in expanding the use of our device.

Another beneficial question to explore is whether our device could be used to differentiate between smaller increments, and values in a much larger range of R_a. Our current device can differentiate between surfaces with values of R_a of 0.05, 0.1, 0.2, 0.4, 0.8, and 1.6 μm. In order to be competitive with current surface roughness measurement devices, we believe that the use of our device would have to be expanded to a set of R_a values beyond its current one. It is possible that our algorithms, or maybe even the entire methodology of using visible light, will break down at some extreme, or some small resolution of values of R_a. Once again, this option could be explored through experimentation.

Both of these paths are steps in expanding the functionality of our device, while also making further strides in transitioning from a proof-of-concept test stand to a practical, fully-marketable product.

CONCLUSIONS

Our team was charged with designing a test stand that proved low-intensity visible light was capable of successfully differentiating between standard R_a values of ground metal surfaces. From functional decomposition, we broke our design into the basic components of light source and sensor. Through a series of experiments, we concluded that the best design would include an LED oriented vertically above the surface of interest, utilizing a pellicle beamsplitter to send the reflected light to a webcam.

The product was refined through further experimentation and design into a compact, easy-to-assemble device, taking the proof-of-concept objective closer to a marketable device. It was manufactured with ABS plastic using rapid prototyping. A user interface was created in LabVIEW, evaluating roughness with an algorithm that binned light intensity and shape to specific R_a values. Further validation testing proved it to be a robust design, capable of significant variations in stand-off distance from the surface of interest.

We thus completed our objective and took further stops toward making a marketable product. If given more time, we would also add an automated calibration procedure to our LabVIEW VI. We would also expand our capabilities beyond just ground surfaces, to other types of machining.

ACKNOWLEDGEMENTS

We would like to acknowledge several people for their help and support throughout this project. It could not have been completed without their invaluable contributions: Section leader Professor Yoram Koren; Customers Hagay Bamberger and En Hong; Expert Consultants Irl Duling, Jeff White, and Chris Megdanoff of Picometrix; GSI Dan Johnson; Professor Reuven Katz; Administrator Julie DeFilippo; Lab Supervisor Steve Erskine; and the other students in Professor Koren's section of ME 450, who often provided groundbreaking insights that furthered the success of our project.

REFERENCES

1. Huynh, Van-Minh and Luk, Francis M. "Method and apparatus for assessing surface roughness." U.S. Patent 4,878,114. 31 October 1989.

2. Seitavuopio, Paulus and Heinämäki, Jyrki and Rantanen, Jukka and Yliruusi, Jouko. "Monitoring Tablet Surface Roughness During the Film Coating Process". AAPS PharmSciTech 2006; 7:2, Article 31.

3. Hennies, Hans-Henning and Kessler, Gunter and Krafft, Gerd and Miller, Georg and Schumacher, Gustav. "Protective coating for turbine blades". U.S. Patent 6,149,389. 21 November 2001.

4. "Engine Blade Coating - Using HVOF in MCrAlY Bond Coating of Turbine Engine Blades by VAC AERO". The A to Z of Materials. 16 July 2009. <C:\Documents and Settings\Derek Geiger\Desktop\ME 450\Engine Blade Coating - Using HVOF in MCrAlY Bond Coating of Turbine Engine Blades by VAC AERO.mht>

5. Howell, Dickon and Behrends, Brigitte. "A review of surface roughness in antifouling coatings illustrating the importance of cutoff length". Biofouling 2006; 22:6, 401 — 410.

6. Sandhu, Gurtej S. and Hudson, Guy. "Method and apparatus for determining surface roughness". U.S. Patent 5,838,445. 17 November 1998.

7. Person, U. (1993). "Roughness measurement of machined surfaces by means of the speckle techniques in the visible and infrared regions." *Optical Engineering*, 32(12), 3327-3332

8. Beckmann, P., Spizzichino, A. *The Scattering of Electromagnetic Waves from Rough Surfaces.* Pergamon Press, New York (1963)

9. Voti, R. L., Leahu, G. L., Gaetani, S., Sibilia, C., Violante, V., Castagna, E., Bertolotti, M. (2009). "Light scattering from a rough metal surface: theory and experiment." *Journal of the Optical Society of America*, 26(8), 1585-1593

10. Bjuggren, M., Krummenacher, L., Mattsson, L. (1997). "Noncontact surface roughness measurement of engineering surfaces by total integrated infrared scattering." *Optical Engineering*, 20(1), 33-45

11. Harvey, J. E., Krywonos, A., Vernold, C. V. (2007). "Modified Beckmann-Kirchhoff scattering model for rough surfaces with large incident and scattering angles." *Optical Engineering*, 46(7), Article 078002

12. Vernold, C.L., Harvey, J. E. (1998). "A Modified Beckmann-Kirchhoff scattering theory for non-paraxial angles." Scattering *and Surface Roughness II – Proceedings of the SPIE*, 3426, 51-56

13. Selvaduray, G. , Amaral, R. A. & Chong, L. H. (2002). Surface Roughness. 6-9.

14. Surface Roughness Measurement Gages. (2002). *Full line of portable, automated & OEM systems providing non-contact measurements* [Brochure]. Prosco Inc.

15. MarSurf WS 1. (2008). *High-precision, non-contact measurement of surface texture using white-light interferometery* [Brochure]. Mahr GmbH.

16. Hong, E. et al, (18 May 2009), "Crankshaft Polish In-Process Inspection," ERC Big Three Quarterly Review Meeting, NSF Engineering Research Center for Reconfigurable Manufacturing Systems.

17. CYH, "Fundamentals of Digital Image Processing," 15.

18. Dym, C. L., Wood, W. H., and Scott, M. J., 2002, “Rank Ordering Engineering Designs: Pairwise Comparison Charts and Borda Counts.”

APPENDIX A

Bill of Materials

Item	Quantity	Part ID #	Cost [USD]	Contact	Notes
1” Diameter Pellicle Beamsplitter	1	NT39-481	145.00	http://www.edmundoptics.com/	Very delicate, read user manual before handling.
Microsoft LifeCam VX-5000	1	8921107	32.99	http://support.microsoft.com/	-
5 MM Purple LED	1	SSL-LX5093VC	0.87	http://www.digikey.com/	May need replacing.
9V Snap Connector	1	270-325	1.99	http://www.radioshack.com/	-
9V Battery	1	23-875	1.99	http://www.radioshack.com/	May need replacing.
DPDT Flatted Metal Lever Toggle Switch	1	275-636	3.99	http://www.radioshack.com/	-
Main Body	1	Part 1, App. E	75.00	http://um3d.dc.umich.edu/hardware/3Dprinter/	Made via rapid prototyping w/ ABS Plastic.
Webcam Door	1	Part 5, App. E	10.00	http://um3d.dc.umich.edu/hardware/3Dprinter/	Made via rapid prototyping w/ ABS Plastic.
Beamsplitter Compartment Door	1	Part 3, App. E	15.00	http://um3d.dc.umich.edu/hardware/3Dprinter/	Made via rapid prototyping w/ ABS Plastic.
Electronics Compartment Door	1	Part 4, App. E	10.00	http://um3d.dc.umich.edu/hardware/3Dprinter/	Made via rapid prototyping w/ ABS Plastic.
Beamsplitter Holder Frame	1	Part 2, App. E	10.00	http://um3d.dc.umich.edu/hardware/3Dprinter/	Made via rapid prototyping w/ ABS Plastic.
10 KΩ Resistor	2	271-1335	0.20	http://www.radioshack.com/	-
3 KΩ Resistor	1	271-1328	0.20	http://www.radioshack.com/	-
Alligator Clips	2	270-380	2.79	http://www.radioshack.com/	-
1” x 1” AR Window	1	NT48-923	13.00	http://www.edmundoptics.com/	-
1/4” 2-56 Screws	2	91773A077	0.03	http://www.mcmaster.com/	-
Total	19		323.05		

APPENDIX B

Changes since Design Review #3

The most significant change since Design Review #3 is the addition of a protective window to the beamsplitter compartment of the device. This change was suggested by our customer, Dr. Hagay Bamberger, with the intention of protecting the delicate pellicle membrane. This antireflective (AR) window is shown in the bill of materials above and in Appendix A.

We also switched from a push on/off switch to a toggle switch for the LED circuit to make it easier for the user to determine the status of the device. The drawing files in Appendix E have been updated to accommodate this change.

Since DR3, we decided to turn the intended circuit board into a series of resistors totaling 23kΩ. The battery is connected to the circuit through a snap-on battery terminal, and one of the leads from the terminal is soldered to the switch. The other lead ends in an alligator clip that clips to the anode of the LED, such that the LED is changeable. The cathode of the LED is connected via alligator clip to the resistance, which is soldered to the switch to complete the circuit.

Though plans were in place to provide a means of level, reliable support for our device, it remains freely portable and can be supported by a simple ring stand if need be.

APPENDIX C

Functional, Manufacturing, and Environmental Material Selection

Material Selection – Functional Performance

For our one of a kind prototype it was rather clear that rapid prototyping was the optimum method of fabrication. With the resources available to us here at the University, we only had two options: a brittle plaster powder ($0.20 per cc) or ABS plastic ($0.40 per cc). We chose the latter for its strength and machining capabilities.

However, when designing a final product intended for market, we had to look much more carefully at potential materials and fabrication methods. The tool that we utilized to do this is CES EduPack 2009. This software is essentially a huge database of materials and manufacturing processes. The user can specify limits for various properties and the software will keep track of the materials that meet the criteria, as well as will show what processes may be performed to the materials. Table C.1 shows the limits that we used for our design.

Table C.1: CES Parameters for the final design.

Parameter	Minimum	Maximum	Unit
Price	0	1.3	$/lb
Max Service Temperature	120	-	°F
Min Service Temperature	-	50	°F
Electrical Resistivity	1×10^6	-	μohm.cm
Transparency	Opaque		-
Water Resistivity	Excellent		-
CO2 Footprint of Production	0	4	lb/lb
Recyclable	Yes		

From the table one can see that we are concerned with price, durability, optical properties, and environmental effects. We want a device that will cost at most a few dollars of material. Also, it must operate in temperatures that will be expected in a typical manufacturing line, so the maximum should be above 120°F and the minimum should be below 50°F. The material should be able to resist water and it should not conduct any electricity from the circuitry in the top compartment. Moreover, we tried to minimize adverse effects on the environment by limiting the carbon footprint of production to a rather low value (4 lb/lb) and by making our product out of a recyclable material. The list of materials that fit these criteria is shown in Figure C.1, ranked by price.

Figure C.1: All materials fitting our selection criteria

Name	Price (USD/lb)
PS (high impact)	0.649 - 0.714
EVA (12% Vinyl acetate, Shore A95/D50)	0.671 - 0.738
EVA (25% Vinyl acetate, Shore A85)	0.68 - 0.748
PET (unfilled, semi-crystalline)	0.689 - 0.758
EVA (33% Vinyl acetate, Shore A65)	0.689 - 0.758
TPO (PP+EP(D)M, Shore 50D)	0.789 - 0.868
TPO (PP+EP(D)M, Shore 55A)	0.789 - 0.868
TPO (PP+EP(D)M, Shore 60D)	0.789 - 0.868
TPO (PP+EP(D)M, Shore 75A)	0.789 - 0.868
TPO (PP+EP(D)M, Shore 90A/40D)	0.789 - 0.868
PS (high impact, flame retardant)	0.839 - 0.923
ASA/PVC (unfilled)	0.875 - 0.963
PB (film)	0.948 - 1.04
PB (extrusion)	0.948 - 1.04
ABS (medium-impact, injection molding)	0.948 - 1.15
ABS (heat resistant, injection molding)	0.948 - 1.3
PB (adhesive resin)	0.948 - 1.04
ASA (extrusion, injection and blow molding)	0.962 - 1.06
ABS (extrusion)	0.989 - 1.09
ABS (rubber modified, injection molding and extrusion)	0.998 - 1.35
ABS (high-impact, injection molding)	1.1 - 1.5
PVC (chlorinated, molding and extrusion)	1.19 - 1.31
PBT (general purpose)	1.22 - 1.34
ABS (flame retarded, molding and extrusion)	1.29 - 1.45

Figure C.2: Manufacturing processes for high impact polystyrene.

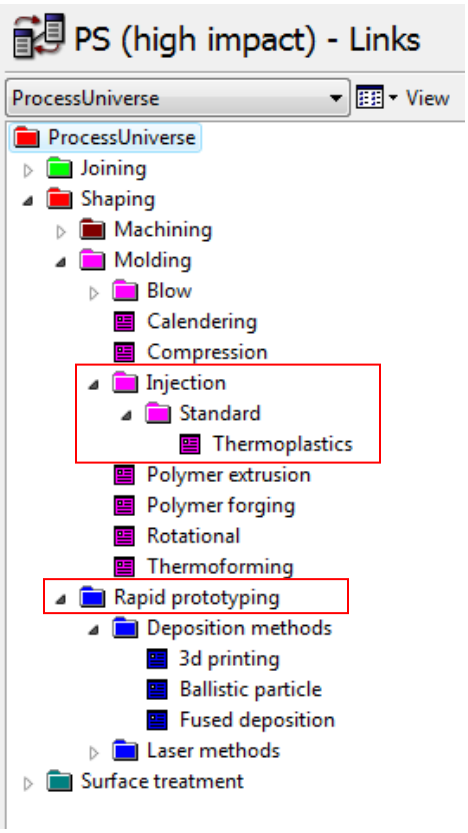

From Figure C.1 one can see that the cheapest material that fit our criteria was HIPS, or high impact polystyrene. This is a low density (0.038 lb/in^3) polymer with impact modifiers for greater impact resistance. This material allows our device to be light, cheap, durable and environmentally friendly. In fact, with this material our device would weigh 0.4 lbs (with no components) and would cost $0.28 of material. This material is often used to make toys and household appliances, and it does not deform very easily (E = 3 x 10^5 psi).We feel that this would be the best material to use for the main block and all the doors – every part that is not directly bought as a component.

Manufacturing Process Selection

Another great feature of the CES software is that it suggests manufacturing processes that are compatible with materials in its database. The CES process suggestions for HIPS can be seen in Figure C.2. Most of the processes shown would not be suitable for our device. All common machining processes (such as milling, turning, drilling, etc) would not be adequate for making our device. These processes would not be able to make such intricate detail on such a small scale while keeping tight tolerances. Thus, we eliminated these processes from our palate. Also, most methods of molding would also not work with our device as it is currently designed. Processes such as blow molding, polymer extrusion, rotational molding, or polymer forging are not able to create very detailed shapes with multiple compartments. We were left with thermoplastic injection molding and rapid prototyping.

The decision between these fabrication methods then comes down to the market size and the amount of fabrication we intend to undertake. Injection molding has very high initial tooling costs (from $3,000 to

$90,000 for a mold) but can produce many units very quickly (60 to 3000 per hour) for low additional cost. Rapid prototyping, on the other hand, has low tooling costs ($40 - $90) but these costs are recurrent for every unit. Also, the production rate is only 0.02 – 0.5 units per hour. Thus, for small production sizes, we would rapid prototype our device in polystyrene. However, if we were to sell about 10,000 units or more we would use thermoplastic injection molding for fabrication.

Material Selection – Environmental Performance

When designing for environmental impact alone, there are many different factors to consider, and a comparison of different materials against these factors can yield a wide variety of results in total emissions; relative impacts in disaggregated damage categories; human health, eco-toxicity, and resource categories; and also in an overall comparison score. The following figures compare our rapid prototyping material (ABS I) to our planned mass production material (HIPS). In the interest of being green, this particular HIPS has been recycled.

Figure C.3: Total Mass Comparison of Materials Consumed and Emitted

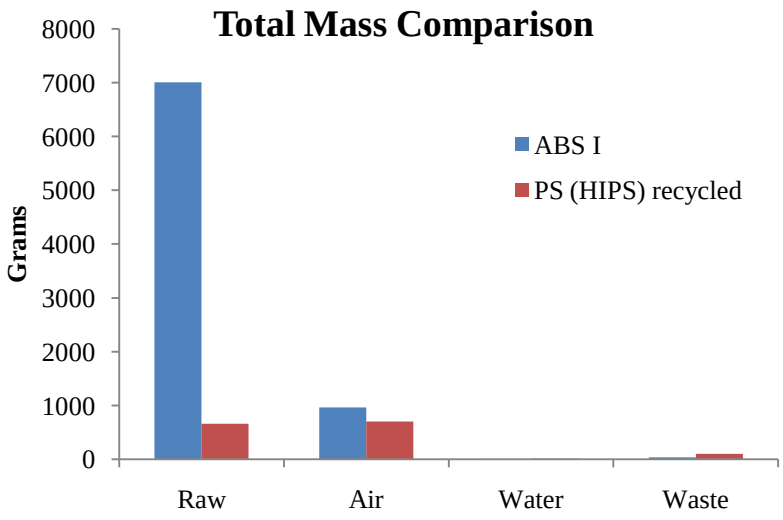

Figure C.4: Relative Impacts in Disaggragated Damage Categories

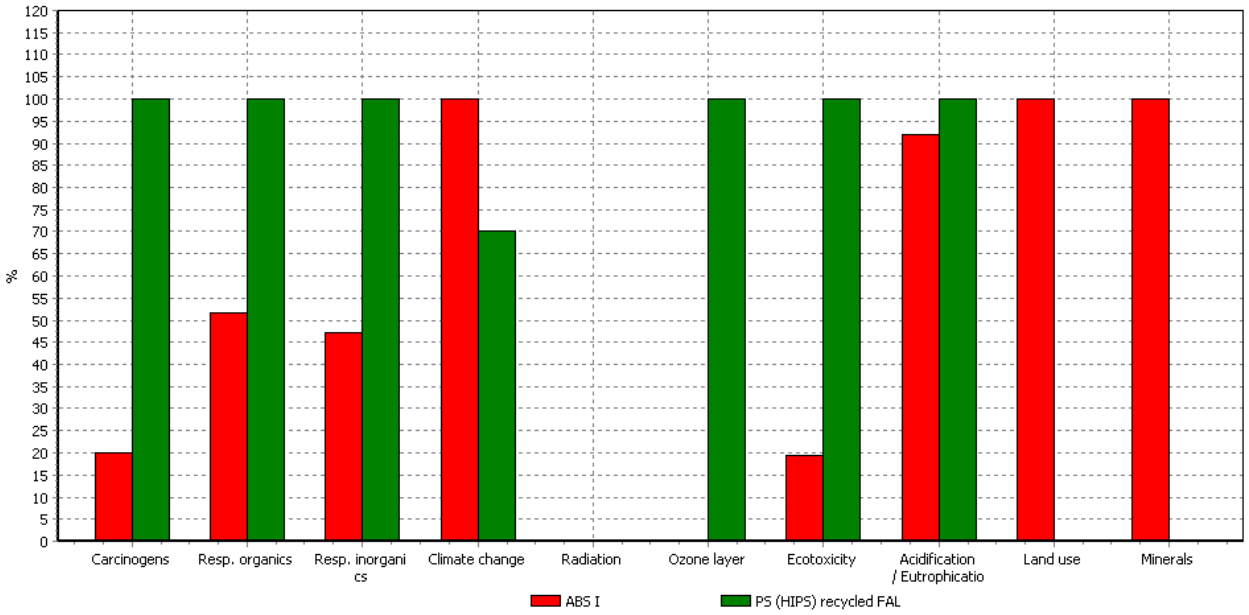

Comparing 0.307 kg 'ABS I' with 0.316 kg 'PS (HIPS) recycled FAL'; Method: Eco-indicator 99 (I) V2.02 / Europe EI 99 I/I / characterization

Figure C.5: Normalized Score in Human Health, Eco-toxicity, and Resource Categories

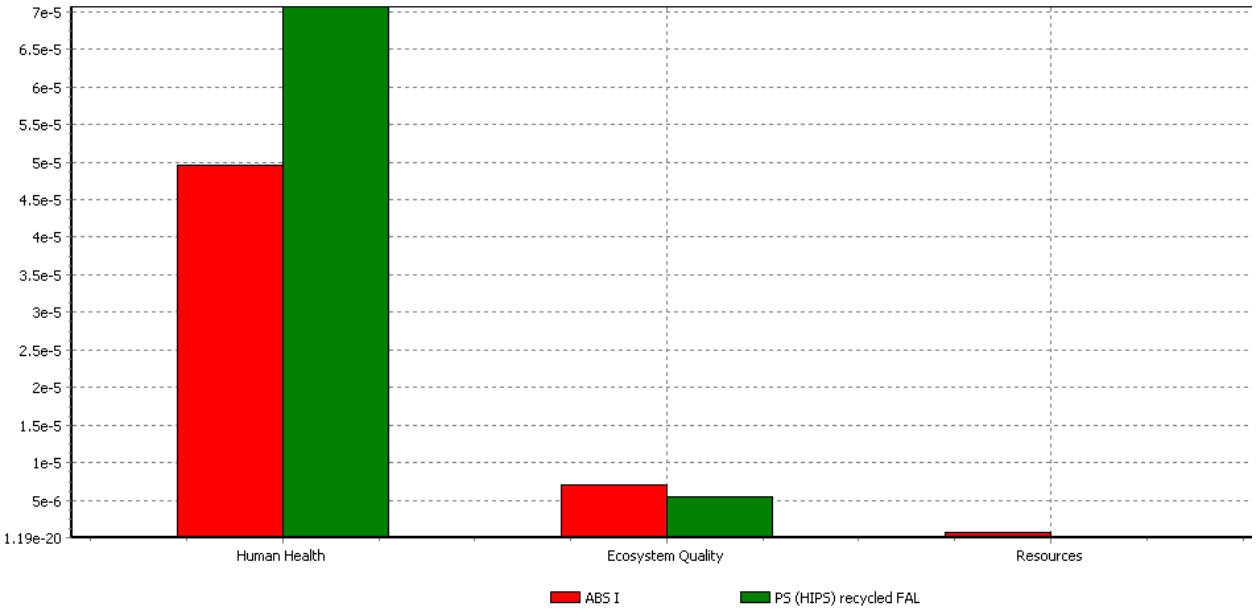

Comparing 0.307 kg 'ABS I' with 0.316 kg 'PS (HIPS) recycled FAL'; Method: Eco-indicator 99 (I) V2.02 / Europe EI 99 I/I / normalization

Figure C.6: Single Score Comparison, showing ABS to be the safer choice

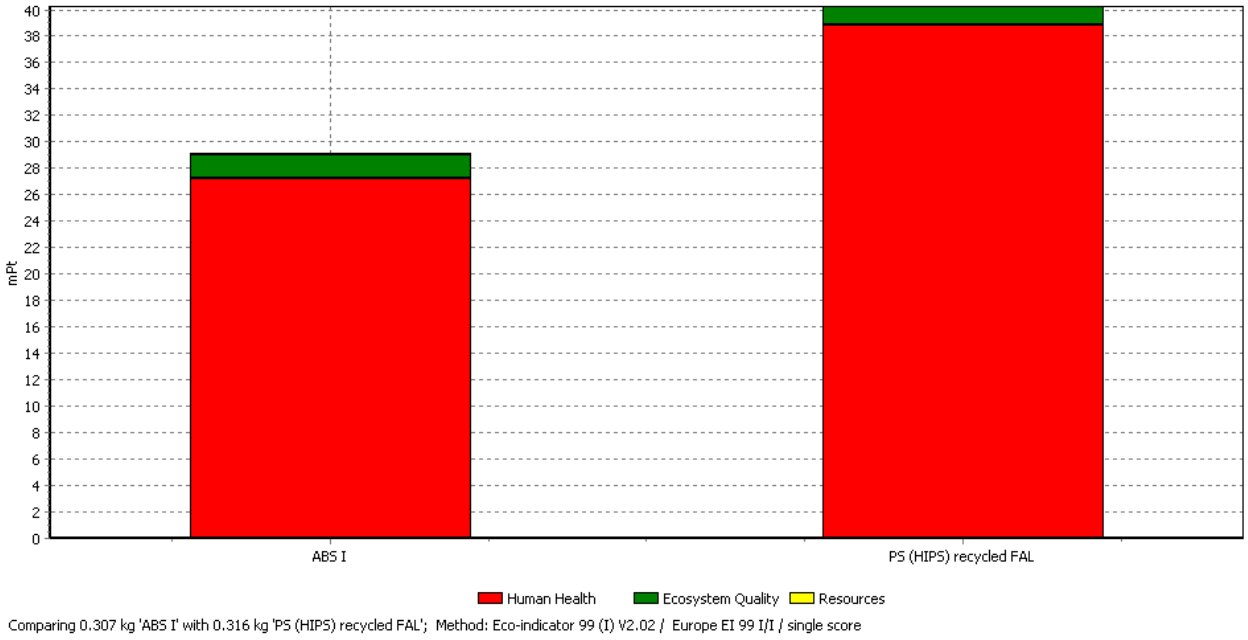

ABS has a higher environmental impact, mostly because it is not recycled, like the example of Polystyrene here. Polystyrene, however, is more dangerous to human health, which trumps the environmental impact according to the above criteria. Due to pricing, though, PS is still a viable option, and as long as proper steps are taken in the manufacturing process to minimize exposure to harmful carcinogens, we should expect little to no devastating results.

Polystyrene (high impact)

General properties

Designation

HIPS, High Impact Polystyrene

Density	0.0372	-	0.0383	lb/in^3
Price	0.649	-	0.714	USD/lb

Tradenames

Aim; Austrex; Avantra; Bapolan; Barlo; Cosden; DaicelStyrol; Diarex; Dicstyrene; Doki; Dunastyr; Dylene; Edistir; Empera; Estastir; Estmec; Estyrene; Extir; Farralloy; Ferroflo; Fiberfil; Fina; Hanapor; Hanarene; Highlac; Hiloy; HKPetro; Kanelite; KanePearl; Kaofulex; Krasten; Lacqrene; Ladene; Lastirol; LGStrene; LusepAPI; Lustrex; MK-Styrol; Nippi; Novacor; NSC; Owispol; Palstyrol; Permastat; Perstyr; Polidesa; Polyflam; PolyRex; Poly-Star; Polystyrol; Porene; Raflite; Replay; Resirene; Rexirene; Shuang Li; Solaroy; Starene; Stirofor; Stirolan; Styroblend; Styrodur; Styrofoam; Styrolen; Styrolux; Styron; Styron A-Tech; Sumibrite; Suprene; Tairirex; TerraWave; Toporex; Trycite; Umastyr; Uniclear; Valtra; Verex

Composition overview

Composition (summary)

blend of (CH(C6H5)-CH2)n + rubber

Base	Polymer			
Polymer class	Thermoplastic : amorphous			
Polymer type	PS-HI			
% filler	0			%
Filler type	Unfilled			

Composition detail

Polymer	80	-	95	%
Impact modifier	5	-	20	%

Mechanical properties

Young's modulus		0.168	-	0.37	10^6 psi
Compressive modulus	*	0.16	-	0.37	10^6 psi
Flexural modulus		0.16	-	0.389	10^6 psi
Shear modulus	*	0.0567	-	0.132	10^6 psi
Bulk modulus	*	0.42	-	0.441	10^6 psi
Poisson's ratio		0.397	-	0.418	
Shape factor		7.7			
Yield strength (elastic limit)		2.76	-	6	ksi
Tensile strength		2.9	-	6.19	ksi
Compressive strength	*	3.31	-	7.21	ksi
Flexural strength (modulus of rupture)		4.55	-	10	ksi
Elongation		40	-	65	%
Hardness - Vickers		5.7	-	12.4	HV
Hardness - Rockwell M	*	38	-	42	
Hardness - Rockwell R		50	-	82	
Fatigue strength at 10^7 cycles	*	1.16	-	2.48	ksi
Fracture toughness	*	0.91	-	2.69	ksi.in^1/2
Mechanical loss coefficient (tan delta)	*	0.0157	-	0.0364	

Impact properties

Impact strength, notched 23 °C	3.49	-	5.52	ft.lbf/in^2
Impact strength, notched -30 °C	1.92	-	3.21	ft.lbf/in^2
Impact strength, unnotched 23 °C	43.9	-	95.2	ft.lbf/in^2
Impact strength, unnotched -30 °C	21.8	-	95.2	ft.lbf/in^2

Thermal properties

Glass temperature	185	-	210	°F
Heat deflection temperature 0.45MPa	176	-	201	°F
Heat deflection temperature 1.8MPa	165	-	194	°F
Maximum service temperature	158	-	194	°F

Minimum service temperature	* -63.4	-	-27.4	°F
Thermal conductivity	0.0751	-	0.11	BTU.ft/h.ft^2.F
Specific heat capacity	* 0.43	-	0.525	BTU/lb.F
Thermal expansion coefficient	43.3	-	45.1	µstrain/°F
Vicat softening point	183	-	208	°F
Processing properties				
Linear mold shrinkage	0.4	-	0.7	%
Melt temperature	351	-	525	°F
Mold temperature	95	-	131	°F
Molding pressure range	9.98	-	20	ksi
Electrical properties				
Electrical resistivity	* 5.98e21	-	5.38e22	µohm.cm
Dielectric constant (relative permittivity)	* 3	-	3.2	
Dissipation factor (dielectric loss tangent)	* 0.001	-	0.006	
Dielectric strength (dielectric breakdown)	* 429	-	515	V/mil
Comparative tracking index	275	-	575	V
Optical properties				
Transparency	Opaque			
Absorption, permeability				
Water absorption @ 24 hrs	0.05	-	0.07	%
Water vapor transmission	0.713	-	1.44	g.mm/(m².day)
Permeability (O2)	156	-	163	cm³.mm/(m².day.atm)
Durability: flammability				
Flammability	Highly flammable			
Durability: fluids and sunlight				
Water (fresh)	Excellent			
Water (salt)	Excellent			
Weak acids	Acceptable			
Strong acids	Limited use			
Weak alkalis	Excellent			
Strong alkalis	Limited use			
Organic solvents	Unacceptable			
UV radiation (sunlight)	Poor			
Oxidation at 500C	Unacceptable			
Primary material production: energy, CO2 and water				
Embodied energy, primary production	9.32e3	-	1.07e4	kcal/lb
CO2 footprint, primary production	3.04	-	3.36	lb/lb
Water usage	2.99e3	-	8.94e3	in^3/lb
Material processing: energy				
Polymer molding energy	* 1.11e3	-	1.22e3	kcal/lb
Polymer extrusion energy	* 429	-	475	kcal/lb
Polymer machining energy (per unit wt removed)	* 215	-	237	kcal/lb
Material processing: CO2 footprint				
Polymer molding CO2	* 0.816	-	0.904	lb/lb
Polymer extrusion CO2	* 0.317	-	0.35	lb/lb
Polymer machining CO2 (per unit wt removed)	* 0.158	-	0.175	lb/lb
Material recycling: energy, CO2 and recycle fraction				
Recycle	True			
Embodied energy, recycling	* 3.99e3	-	4.41e3	kcal/lb
CO2 footprint, recycling	* 1.28	-	1.41	lb/lb
Recycle fraction in current supply	5.7	-	6.3	%
Downcycle	True			
Combust for energy recovery	True			
Heat of combustion (net)	* 4.36e3	-	4.58e3	kcal/lb
Combustion CO2	* 3.29	-	3.45	lb/lb

Landfill	True
Biodegrade	False
A renewable resource?	False

Notes

Typical uses

Toys; light diffusers; beakers; cutlery; general household appliances; video/audio cassette cases; electronic housings; refrigerator liners.

Reference sources

Data compiled from multiple sources. See links to the References table.

APPENDIX D

Quality Functional Deployment (QFD) Diagram

Weight (-)															
Length (-)		++													
Width (-)		++													
Height (-)		++													
Angle of incidence of light (-)			+	+	-										
Lightsource dispersion						+									
Optical sensor resolution (+)															
Strength of Materials (+)		+													
Light intensity (+)								+							
Light wavelength (-)								-							
Time of Measurement (-)								-							
Signal-to-Noise Ratio (+)						+	+	+		+	+				
Steps in Operation (-)												+			
Distance from sample					+	--		-		++					
Customer Needs	**Customer Weights**	Weight (-)	Length (-)	Width (-)	Height (-)	Angle of incidence of light (-)	Lightsource dispersion	Optical sensor resolution (+)	Strength of Materials (+)	Light intensity (+)	Light wavelength (-)	Time of Measurement (-)	Signal-to-Noise Ratio (+)	Steps in Operation (-)	Distance from sample
Easy Movable / Portable	3	9	3	3	3										
Capable of differentiating between 0.1, 0.2, 0.4, 0.8, 1.6 µm	5					1	9	9		3	9		3		3
Repeatability	4					1	9	9		3	1		3		3
Capable of Measuring a Sample Area of 200 mm^2	5		3	3	1	1	9			3					9
Low Cost of Implementation	4		1	1	1		3	9	9	3			3		
Durable	3	1	1	1	1				9						
Safe for User and Surrounding Environment	5	9	1	1	1					3	9			3	
Completes Measurements Quickly	4											9	1		
Easily Operable User Interface	4													9	
Aesthetics	1		3	3	3										
Minimized Invasiveness	5					3	1	1		3				1	9
	Raw score	75	39	39	29	29	143	122	63	84	94	36	43	56	117
	Scaled	0.524	0.273	0.273	0.203	0.203	1	0.853	0.441	0.587	0.657	0.252	0.301	0.392	0.818
	Relative Weight	8%	4%	4%	3%	3%	15%	13%	7%	9%	10%	4%	4%	6%	12%
	Rank	6	10	10	13	13	1	2	7	5	4	12	9	8	3
Requirement Benchmarking	Best in Class	0.44	25	19	25				400			100		1	5
	AVE	3	200	160	200				150			2500		2	2
	Worst in Class	200	800	500	450				30			10000		6	0
Technical Requirement Units		kg	mm	mm	mm				Mpa		nm	sec		Steps	mm
Technical Requirement Targets		1	150	150	400	TBD	TBD	High	55	TBD		3	10	1	
Technical Requirement USL		15	600	600	1000			500	200		380	60	100	5	10
Technical Requirement LSL		0.1	5	5	10			50	20		750	0	1	0	1

APPENDIX E

Figure E.1: Assembly Drawing [mm]

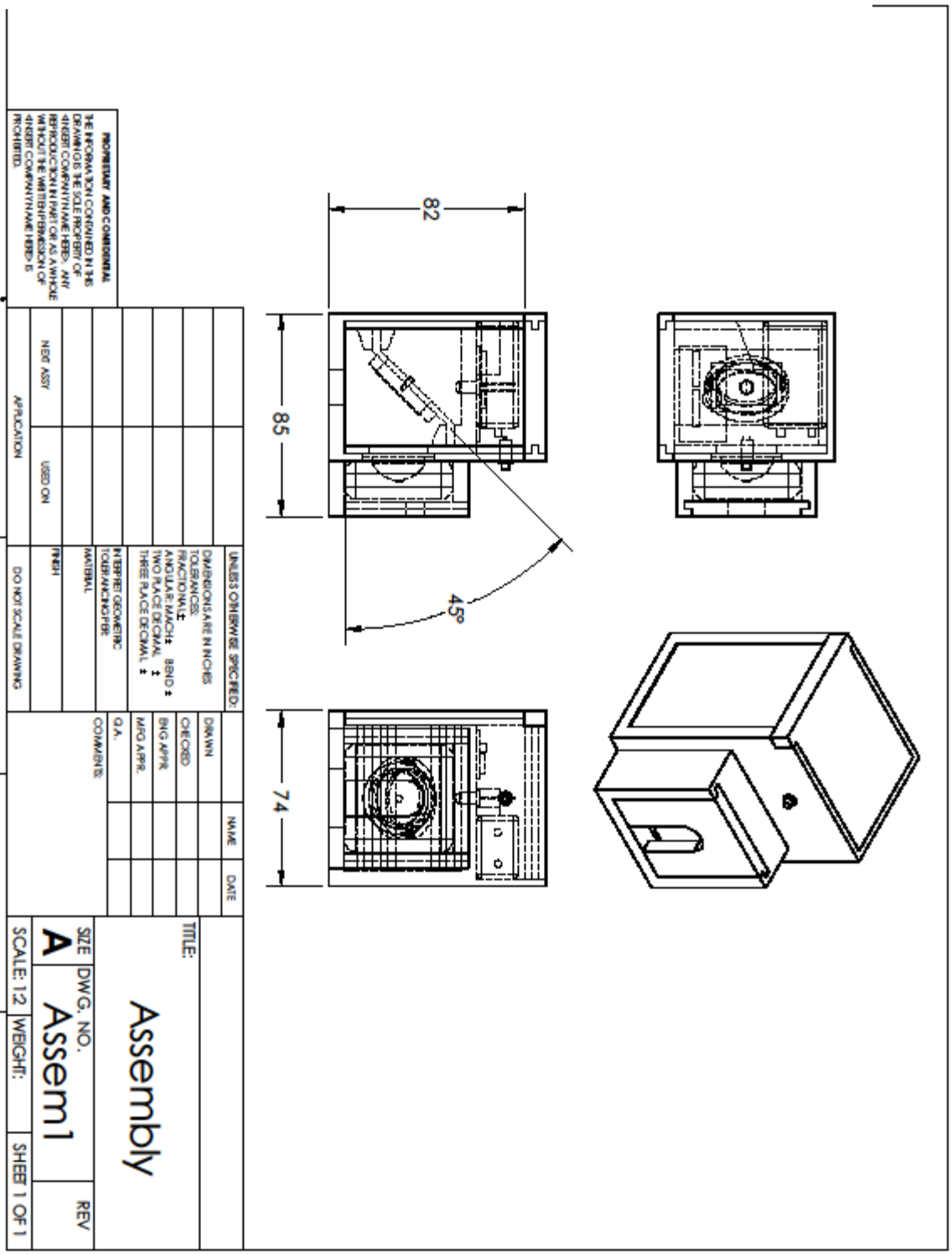

Figure E.2: Main Block Drawing [mm], Part 1

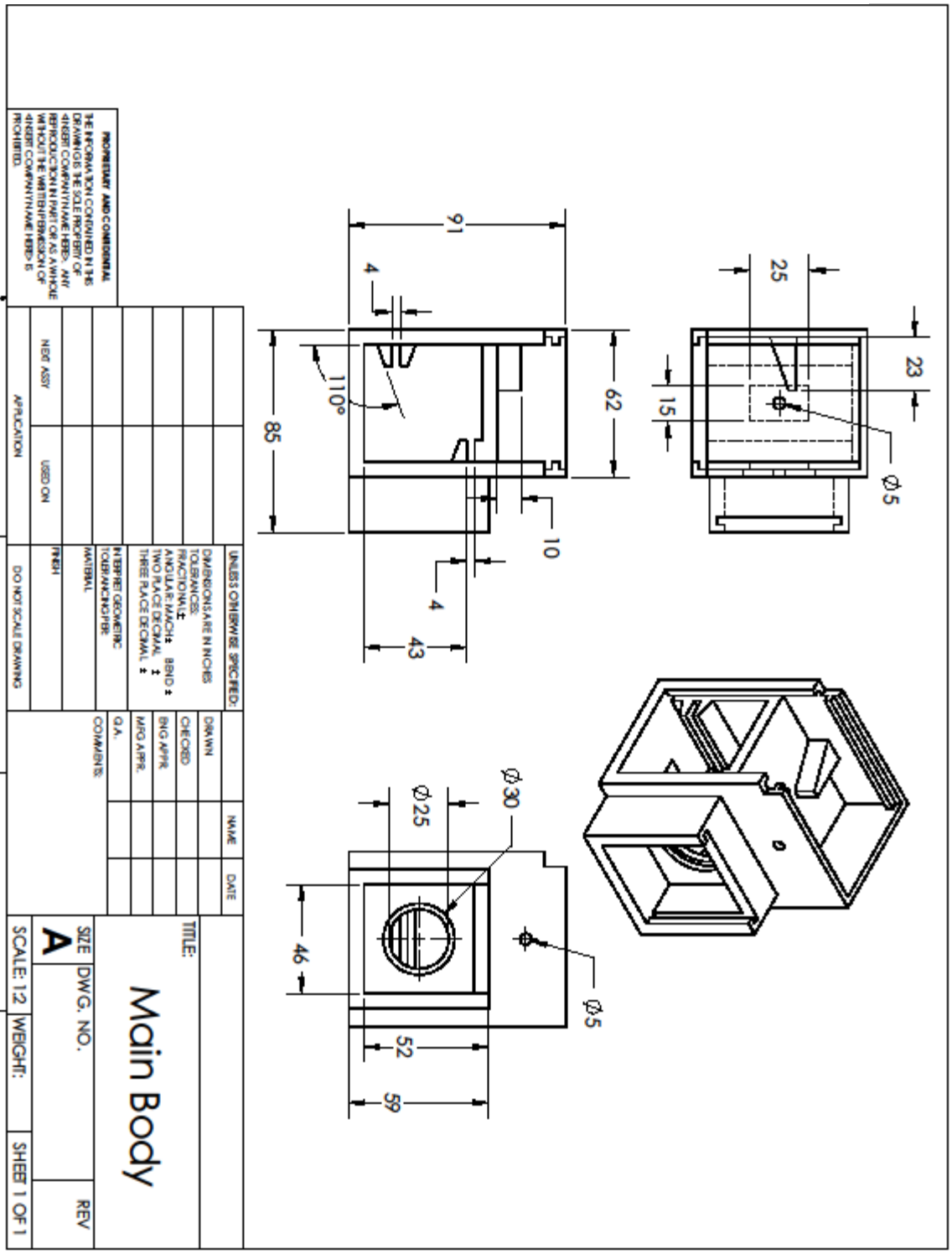

Figure E.3: Beamsplitter Holder Drawing [mm], Part 2

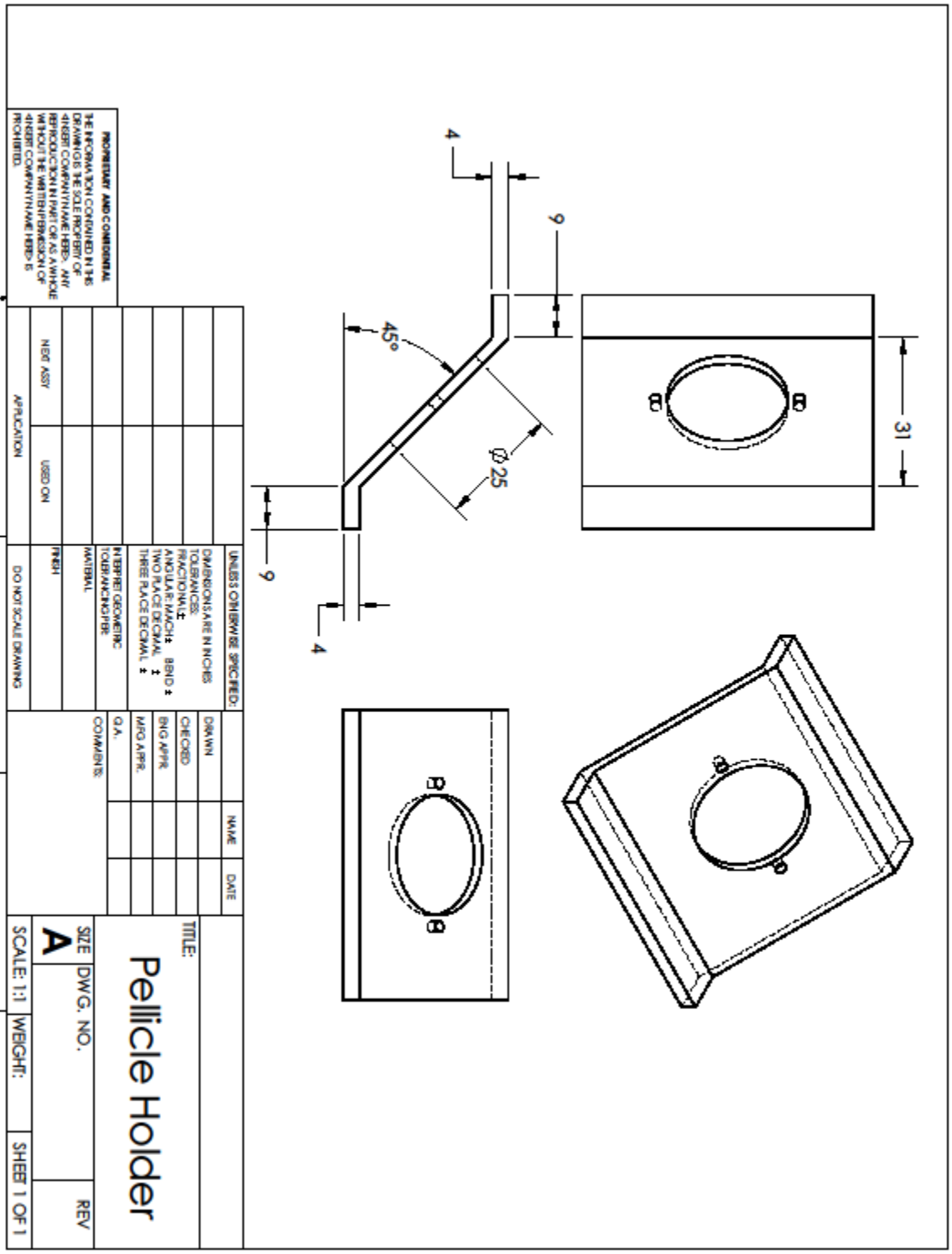

Figure E.4: Pellicle Mirror Drawing [mm]

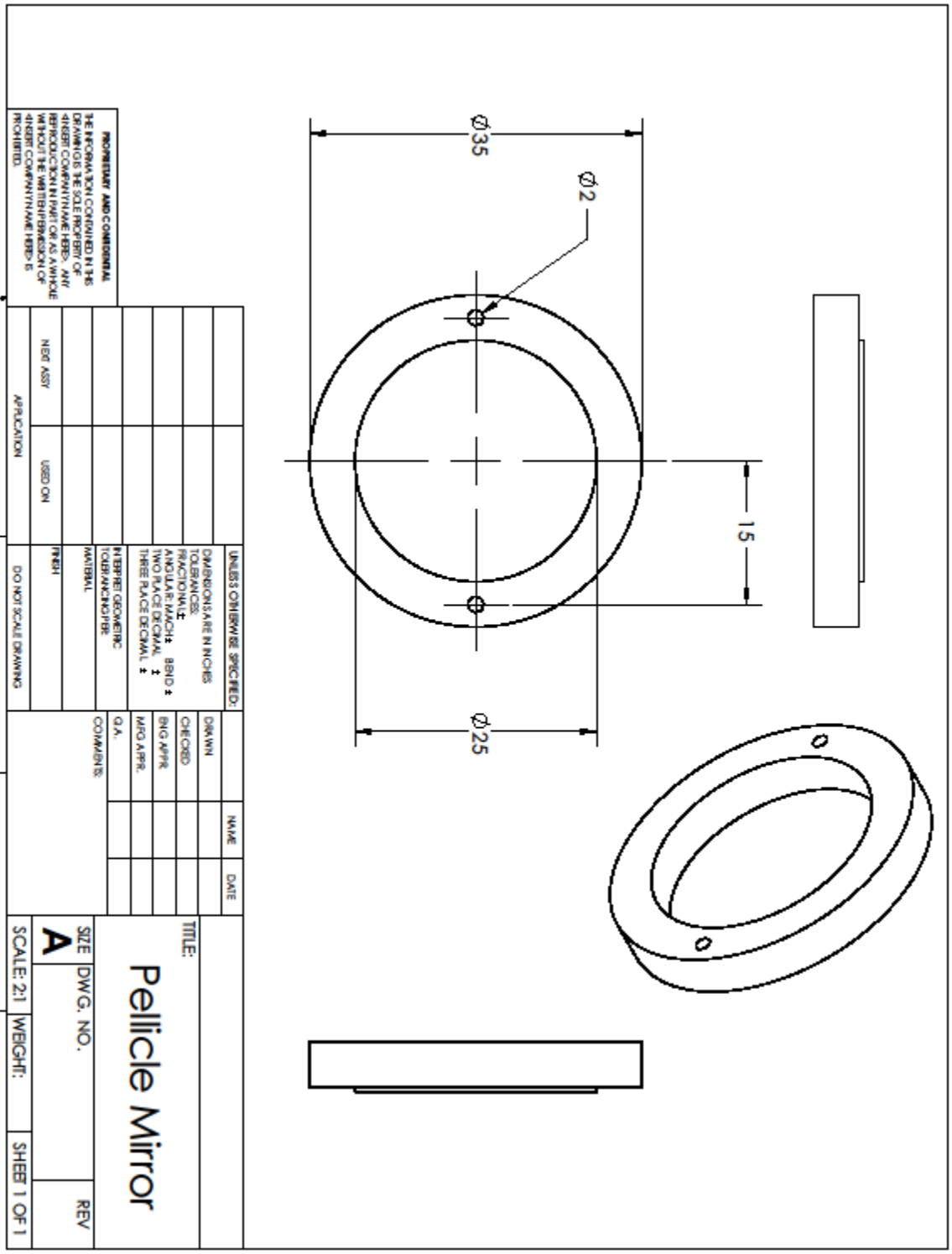

Figure E.5: Beamsplitter Compartment Door Drawing [mm], Part 3

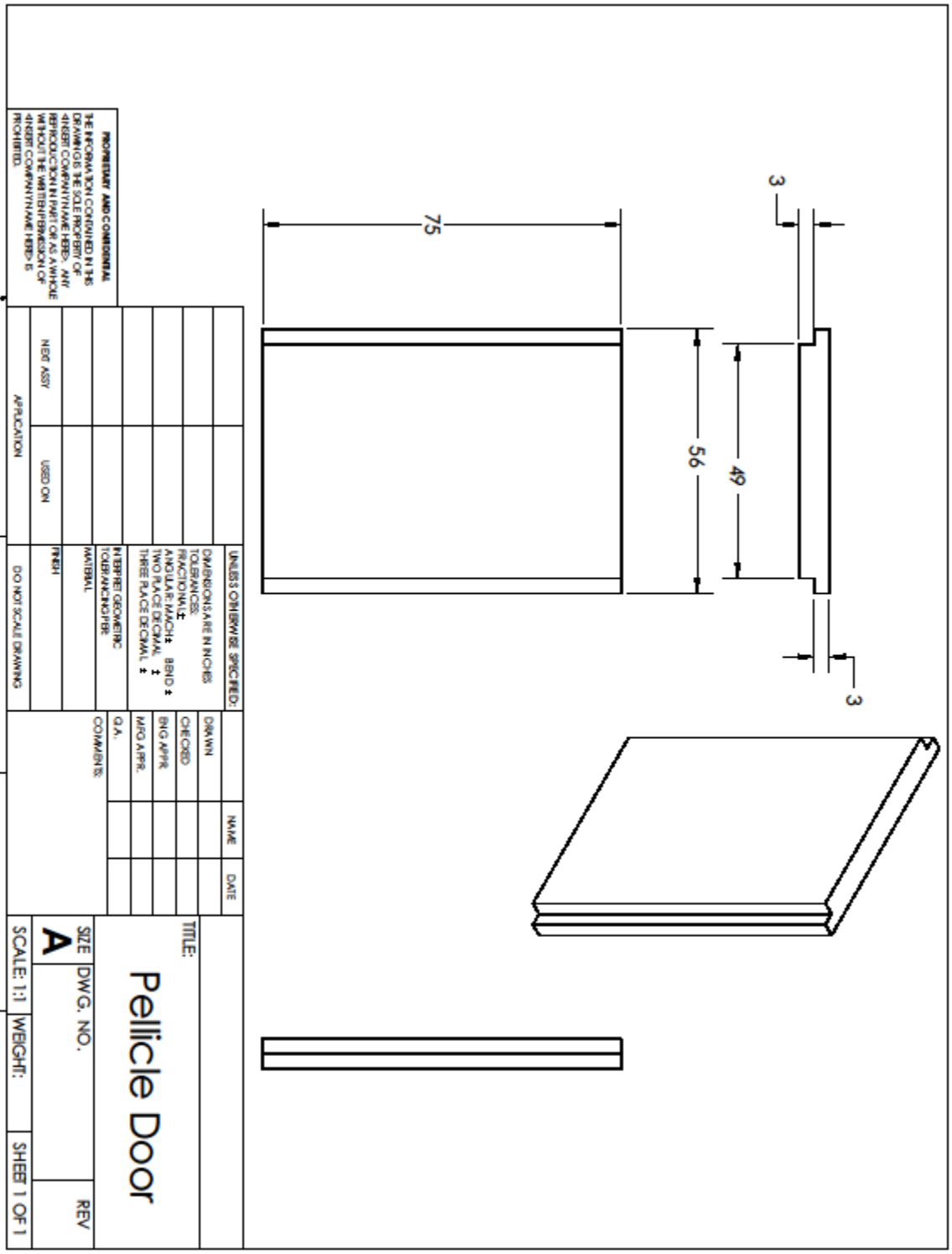

Figure E.6: Battery Cover Drawing [mm], Part 4

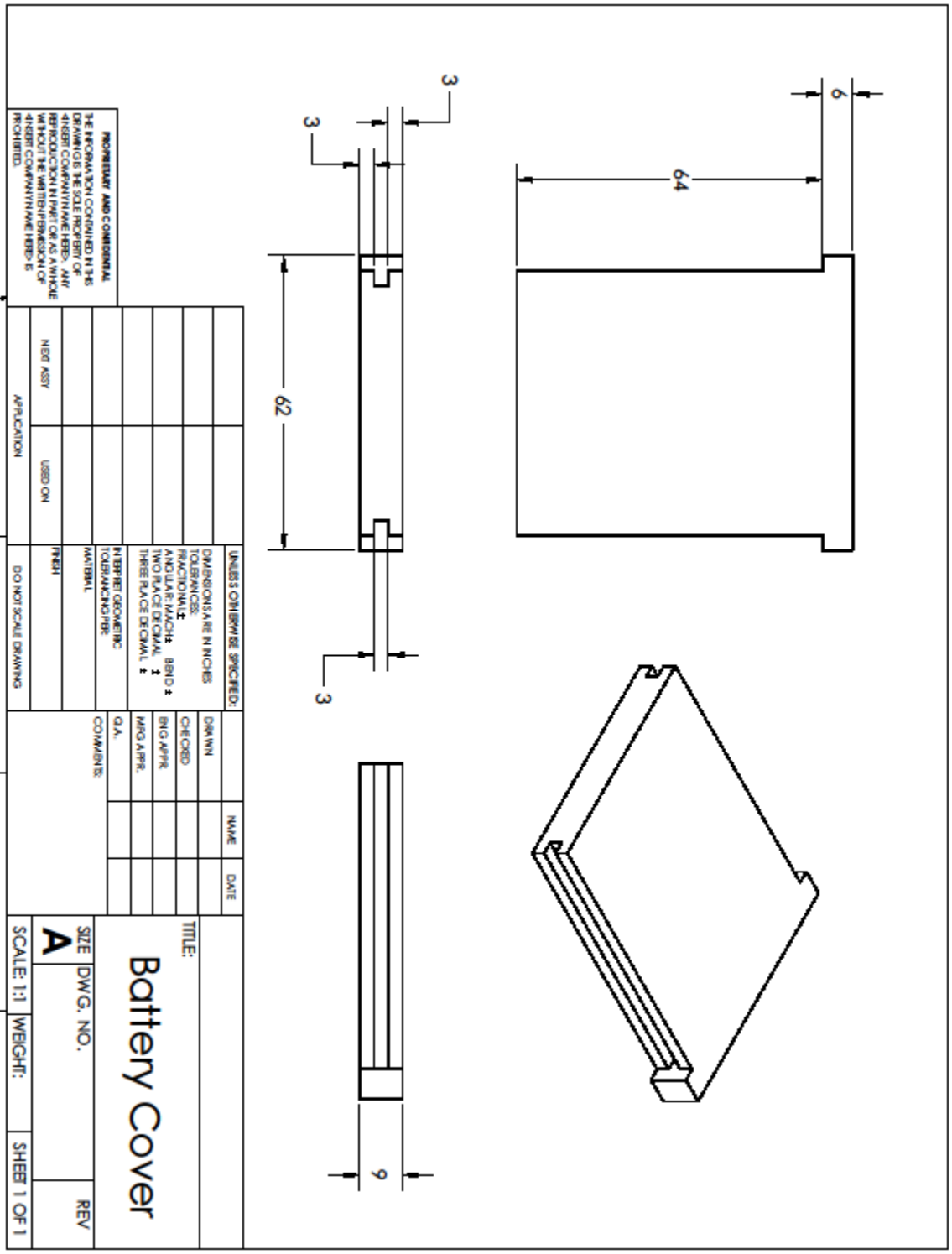

Figure E.7: Camera Compartment Door Drawing [mm], Part 5

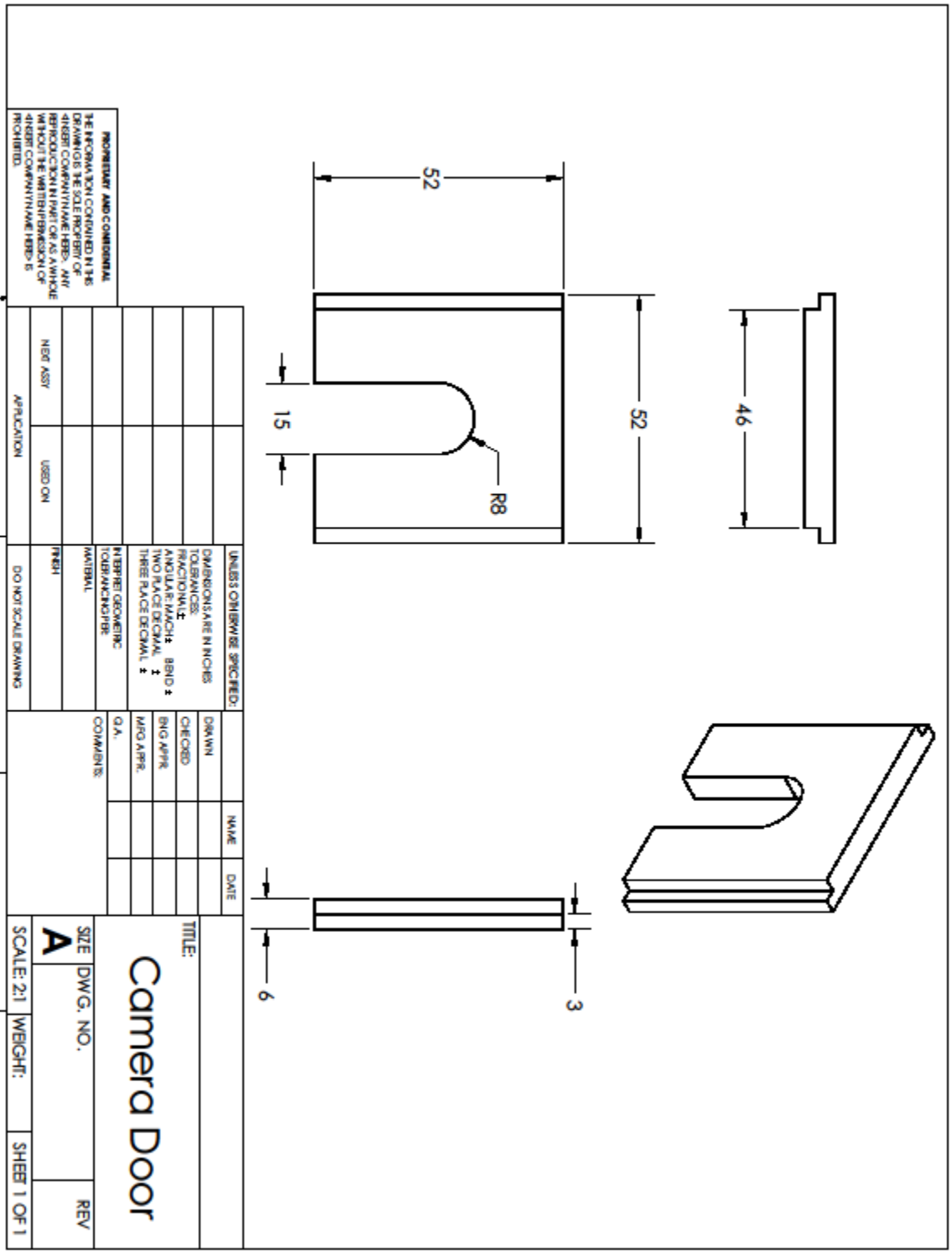

Figure E.8: Webcam Drawing [mm]

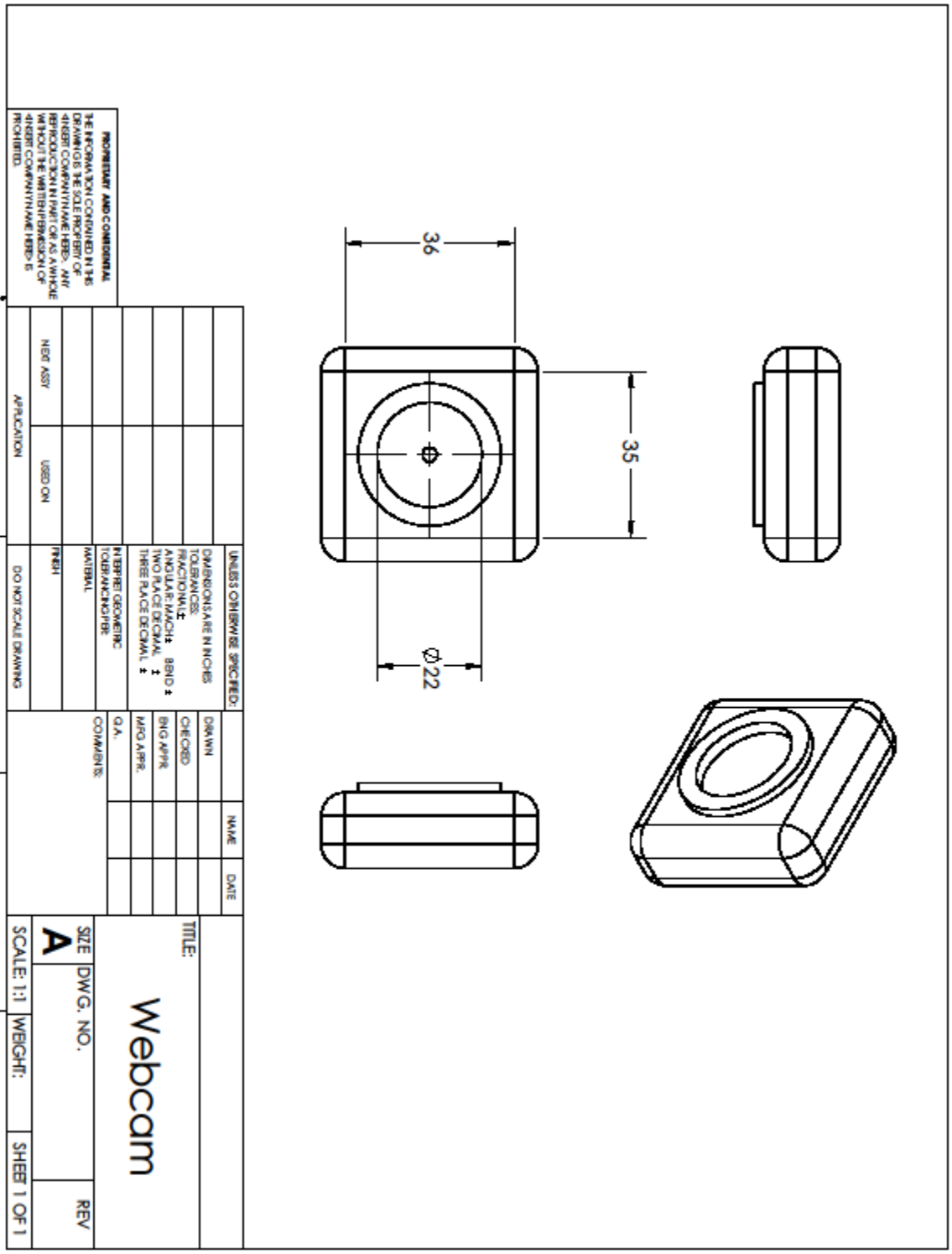

Figure E.9: Purple LED Drawing [mm]

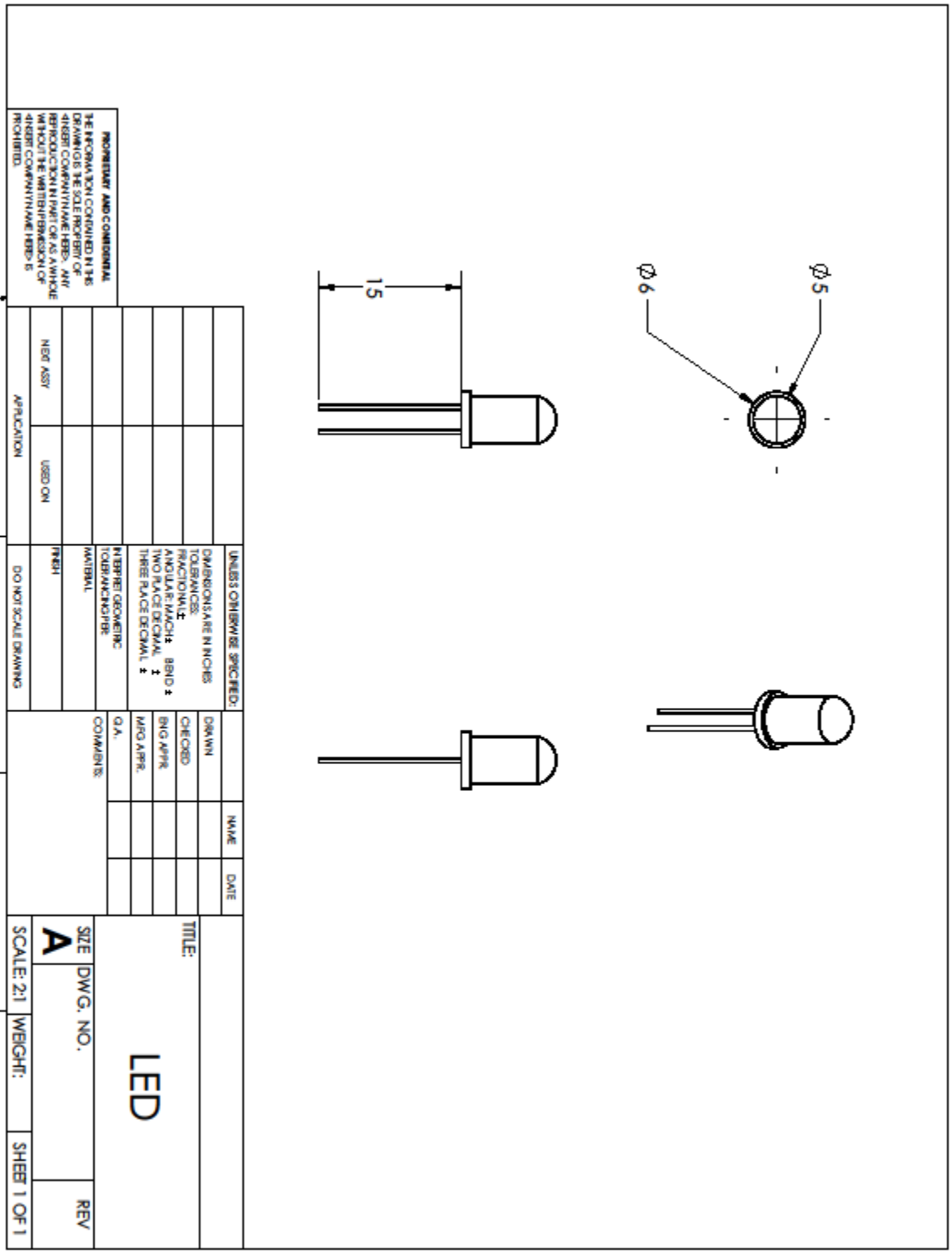

Figure E.10: Switch Drawing [mm]

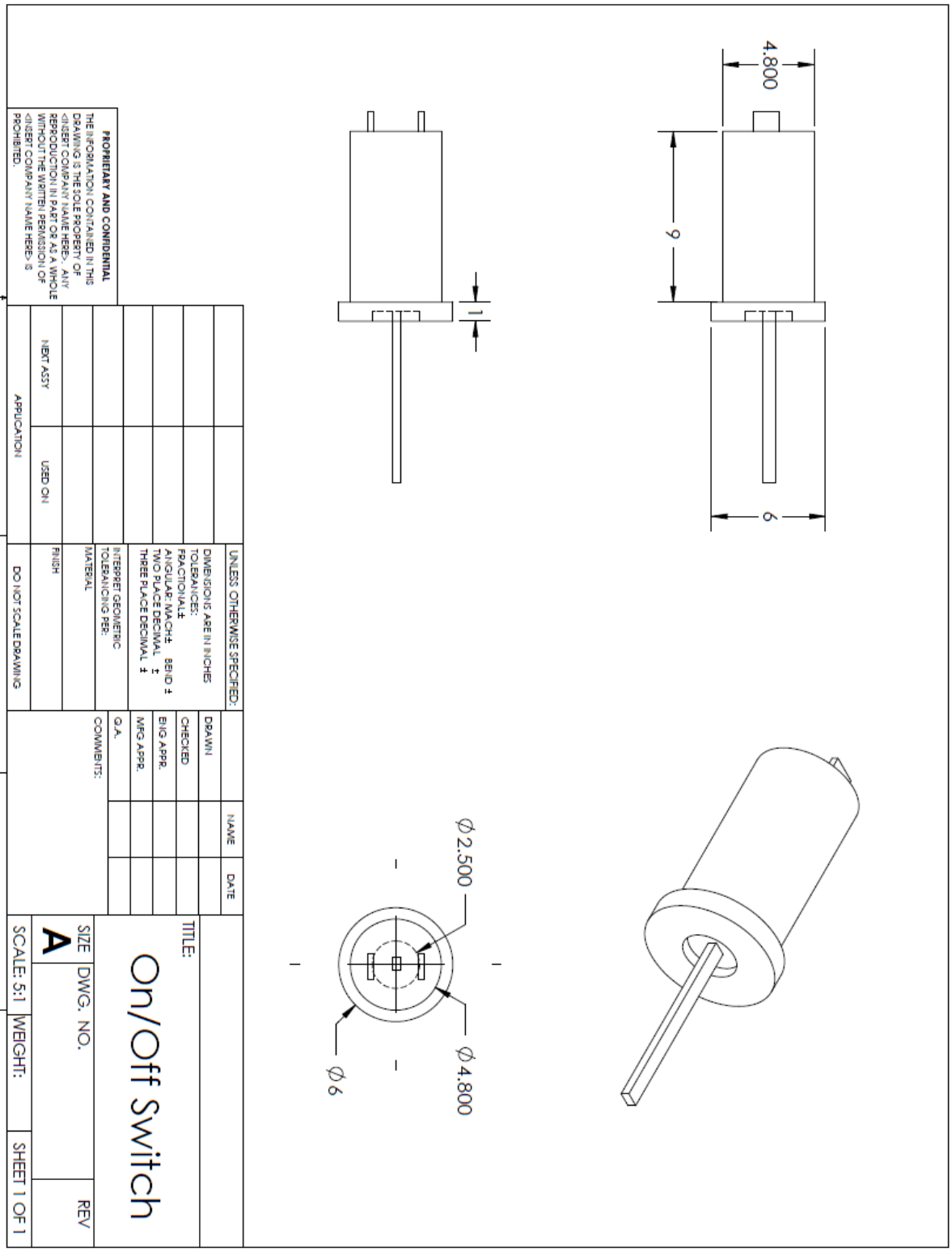

Figure E.15: Stand Apparatus Drawing [mm]